Fungal Genetics and Biology 159 (2022) 103669

Contents lists available at ScienceDirect

Fungal Genetics and Biology

journal homepage: www.elsevier.com/locate/yfgbi

Localisation of phosphoinositides in the grass endophyte *Epichloë festucae* and genetic and functional analysis of key components of their biosynthetic pathway in *E. festucae* symbiosis and *Fusarium oxysporum* pathogenesis

Berit Hassing [a,b,2], Alyesha Candy [a,b], Carla J. Eaton [a,b], Tania R. Fernandes [c,1], Carl H. Mesarich [b,d], Antonio Di Pietro [c], Barry Scott [a,b,*]

[a] School of Fundamental Sciences, Massey University, Palmerston North, New Zealand
[b] Bio-Protection Research Centre, New Zealand
[c] Departamento de Genética, Campus de Excelencia Internacional Agroalimentario ceiA3, Universidad de Córdoba, Córdoba, Spain
[d] School of Agriculture and Environment, Massey University, Palmerston North, New Zealand

ARTICLE INFO

Keywords:
Chemotaxis
Epichloë festucae
Fusarium oxysporum
Phosphoinositides
Plant-fungal interaction
PTEN

ABSTRACT

Phosphoinositides (PI) are essential components of eukaryotic membranes and function in a large number of signaling processes. While lipid second messengers are well studied in mammals and yeast, their role in filamentous fungi is poorly understood. We used fluorescent PI-binding molecular probes to localize the phosphorylated phosphatidylinositol species PI[3]P, PI[3,5]P_2, PI[4]P and PI[4,5]P_2 in hyphae of the endophyte *Epichloë festucae* in axenic culture and during interaction with its grass host *Lolium perenne*. We also analysed the roles of the phosphatidylinositol-4-phosphate 5-kinase MssD and the predicted phosphatidylinositol-3,4,5-triphosphate 3-phosphatase TepA, a homolog of the mammalian tumour suppressor protein PTEN. Deletion of *tepA* in *E. festucae* and in the root-infecting tomato pathogen *Fusarium oxysporum* had no impact on growth in culture or the host interaction phenotype. However, this mutation did enable the detection of PI[3,4,5]P_3 in septa and mycelium of *E. festucae* and showed that TepA is required for chemotropism in *F. oxysporum*. The identification of PI[3,4,5]P_3 in Δ*tepA* strains suggests that filamentous fungi are able to generate PI[3,4,5]P_3 and that fungal PTEN homologs are functional lipid phosphatases. The *F. oxysporum* chemotropism defect suggests a conserved role of PTEN homologs in chemotaxis across protists, fungi and mammals.

1. Introduction

Phosphoinositides (PI) regulate key cellular functions by interacting with proteins that reside in membranes or by recruiting proteins to membranes through PI-binding domains or polybasic amino acid (aa) stretches (Balla, 2013; De Craene et al., 2017). The asymmetric distribution of PIs within organelle membranes defines and maintains membrane identity (De Craene et al., 2017; Falkenburger et al., 2010). PIs consist of a glycerol backbone with two fatty acid chains attached via an ester bond, and a headgroup consisting of phosphate esterified to an inositol ring (Fig. S1). The ring can be phosphorylated or dephosphorylated at positions 3, 4 or 5 by specific kinases and phosphatases, respectively, resulting in seven phosphorylated PI species: PI[3]P, PI[4]P, PI[5]P, PI[3,4]P_2, PI[3,5]P_2, PI[4,5]P_2, PI[3,4,5]P_3 (Balla, 2013; De Craene et al., 2017). To date, only mammals have been shown to produce all seven PIs, while in plants, neither PI[3,4]P_2 nor PI[3,4,5]P_3, and in fungi, neither PI[5]P nor PI[3,4]P_2, have been detected (De Craene et al., 2017).

The most abundant PI is PI[4,5]P_2, which accounts for 30% of the PIs in yeast and 45% in humans, and localizes predominantly at the inner leaflet of the plasma membrane (PM) (De Craene et al., 2017; Di Paolo and De Camilli, 2006). PI[4,5]P_2 plays essential roles in endo- and exocytosis, actin cytoskeleton rearrangement, the activity of ion channels and the establishment of cell polarity (Balla, 2013; De Craene et al.,

* Corresponding author at: School of Fundamental Sciences, Massey University, Palmerston North, New Zealand.
E-mail address: d.b.scott@massey.ac.nz (B. Scott).
[1] Current address: GreenUPorto – Sustainable Agrifood Production Research Centre/Inov4Agro & DGAOT, Faculty of Science, University of Porto, Campus de Vairão, Rua da Agrária 747, 4485-646 Vairão, Portugal.
[2] Current address: Ferrier Research Institute, Victoria University of Wellington, Wellington, New Zealand.

https://doi.org/10.1016/j.fgb.2022.103669
Received 16 November 2021; Received in revised form 15 January 2022; Accepted 27 January 2022
Available online 1 February 2022
1087-1845/© 2022 Elsevier Inc. All rights reserved.

2017). In mammalian cells, PI[4,5]P_2 is generated via phosphorylation of either PI[4]P or PI[5]P by type I phosphatidylinositol 4-phosphate 5-kinases or type II phosphatidylinositol 5-phosphate 4-kinases, respectively. In addition, PI[4,5]P_2 is also produced through dephosphorylation of PI[3,4,5]P_3 by a phosphatidylinositol 3,4,5-trisphosphate 3-phosphatase named PTEN (Phosphatase and TENsin homolog). PTEN acts both as a lipid phosphatase and as a dual specificity tyrosine-, serine- and threonine-protein phosphatase. The lipid phosphatase activity of mammalian PTEN is essential for its role as a tumour suppressor protein, as dephosphorylation of PI[3,4,5]P_3 inhibits the activation of downstream components of the phosphatidylinositol PI3K/AKT pathway (Manning and Cantley, 2007). As a consequence, disruption of PTEN results in deregulated cell proliferation and the onset of cancer (Chen et al., 2018; Liaw et al., 1997).

In fungi, PI[4,5]P_2 can be generated either by a homolog of the mammalian phosphatidylinositol 4-phosphate 5-kinase, Mss-4 (Desrivières et al., 1998; Mähs et al., 2012) or by a homolog of the mammalian PTEN phosphatase (Balla, 2013). This, however, has so far only been shown in *Schizosaccharomyces pombe*, where deletion of the PTEN ortholog *ptn1*, resulted in the accumulation of its substrate PI [3,4,5]P_3. In addition the *ptn1* deletion mutant exhibited misshapen vacuoles and sensitivity to osmotic stress, while in the budding yeast *Saccharomyces cerevisiae* deletion of *TEP1* (homolog of the mammalian *PTEN*) caused mislocalisation of dityrosine during sporulation and increased resistance to the phosphoinositide-3 kinase inhibitor, wortmannin (Heymont et al., 2000; Mitra et al., 2004). In *Fusarium graminearum,* mutants lacking *Fgtep1* (encoding Tep1) displayed reduced conidiation, decreased germination in the presence of wortmannin, and reduced virulence on wheat coleoptiles (Zhang et al., 2010). Similarly, in the corn pathogen *Ustilago maydis,* deletion of *Umptn1* (encoding Ptn1) caused a decrease in teliospore production, germination and virulence (Vijayakrishnapillai et al., 2018).

Here we investigated the role of PI signaling in two plant-infecting filamentous ascomycetes, *Epichloë festucae* and *Fusarium oxysporum*, that display very different lifestyles. In nature, *E. festucae* grows exclusively within host grasses such as *Lolium perenne*, where it establishes a mutually beneficial symbiotic interaction (Schardl, 2001). This endophyte forms an extensive intercellular hyphal network within the aerial tissues of the plant host as well as epiphyllous hyphae on the plant surface (Becker et al., 2016; Chung and Schardl, 1997; Scott and Schardl, 1993). By contrast, *F. oxysporum* resides mainly in the soil, from where it locates and penetrates the roots of host plants to colonize the xylem vessels and cause devastating vascular wilt disease on more than one hundred crops (Dean et al., 2012; Di Pietro et al., 2003). Intriguingly, both the mutualistic and the pathogenic interaction of these two fungi are exquisitely regulated by conserved signaling pathways, including three mitogen-activated protein kinase (MAPK) pathways, the cell wall integrity (CWI), the invasive growth (IG) and the high-osmolarity glycerol (HOG) pathway, the striatin-interacting phosphatase and kinase (STRIPAK) complex, and reactive oxygen species (ROS) signaling (Becker et al., 2015; Di Pietro et al., 2001; Eaton et al., 2008; Green et al., 2016; Segorbe et al., 2017; Tanaka et al., 2006; Turrà et al., 2015). However, the role of PI signaling during the key steps of symbiosis and root infection is currently unknown. Here we studied the localisation of PIs in *E. festucae* using a purpose-designed suite of PI-binding molecular probes. Furthermore, we analysed the role of two key components in PI signaling, the lipid kinase Mss4 and the lipid phosphatase PTEN, during hyphal growth, development and the *E. festucae–L. perenne* interaction, and also tested the role of PTEN in hyphal chemotropism of *F. oxysporum*.

2. Materials and methods

2.1. Bioinformatic and statistical analyses

A tBLASTn analysis against the *E. festucae* Fl1 and the *F. oxysporum* f. sp. *lycopersici* 4287 genome was performed on the Kentucky Endophyte database (endophyte.uky.edu) (Schardl et al., 2013) and the NCBI BLAST server, respectively, using the Tep1 protein sequence from *S. cerevisiae* (*Sc*Tep1) as a query, to identify EfM3.013870 and FOXG_09154 (hereafter referred to as TepA). Expression analysis of *tepA* in *E. festucae* made use of previous transcriptome datasets (Chujo et al., 2019; Eaton et al., 2015). The protein sequence of TepA was analysed with InterProScan (Jones et al., 2014), and protein alignments were generated using MAFFT (Katoh et al., 2017) and JalView (v1.0). Boxplots were generated online with BoxPlotR (available on http://shiny.chemgrid.org/boxplotr/). Dunn's test for multiple comparisons, as implemented in the R package dunn.test v1.3.5 (Dinno, 2017) was used to identify significant differences in the number of hyphae per intercellular space between all deletion and over-expression strains. One-way ANOVAs were used to test for differences in plant phenotypes between wild-type (WT) and overexpression strains. In each case, the ANOVA was fitted with R, and a Bonferroni correction was applied to all *p*-values to account for multiple testing.

2.2. Strains and growth conditions

Escherichia coli and *E. festucae* strains were grown at 37 °C and 22 °C, respectively, as previously described (Green, 2016). All strains are listed in Table S1. Conidia were harvested by scrubbing colonies with sterile water followed by filtering through glass wool as previously described (Green, 2016).

The tomato-pathogenic isolate *F. oxysporum* f. sp. *lycopersici* 4287 (FGSC 9935) was used throughout the study. For extraction of DNA and microconidia production, fungal strains were grown at 28 °C with shaking at 170 rpm in liquid PDB medium supplemented with the appropriate antibiotics as previously described (Di Pietro and Roncero, 1998).

2.3. Plant growth and inoculation

E. festucae strains were inoculated into *L. perenne* seedlings (cv. Samson) and grown as previously described (Becker et al., 2018; Latch and Christensen, 1985).

Tomato root inoculation assays with *F. oxysporum* were performed as previously described (Di Pietro and Roncero, 1998). Roots of 2-week-old *Solanum lycopersicum* seedlings (cv Moneymaker) were immersed for 30 min in a suspension of $5x10^6$ microconidia ml^{-1} and planted in minipots with vermiculite. Plants (ten per treatment) were maintained in a growth chamber (15 h:9h, light:dark cycle, 28 °C). Survival was recorded daily, calculated by the Kaplan-Meier method and compared among groups using the log-rank test.

2.4. DNA analysis, PCR and sequencing

E. festucae genomic DNA was isolated from freeze-dried mycelium, as previously described (Byrd et al., 1990). Plasmid DNA was isolated from *E. coli* liquid cultures using the High Pure plasmid isolation kit (Roche, Basel, Switzerland).

PCR amplification of short fragments for screening purposes (<3 kbp) was conducted using OneTaq® (New England Bolabs (NEB), Ipswich, USA) polymerase and of long fragments (>3 kbp) for subsequent cloning procedures using Phusion Polymerase (Thermo Fischer, Waltham, USA). PCR fragments were separated by agarose-gel electrophoresis on a 0.8% (w/v) gel, and gel extractions were performed with the Wizard SV Gel and PCR clean-up kit (Promega, Madison, USA). Sequencing of plasmids was performed at the Massey Genome Centre. Sequence data was analysed and assembled (ClustalW) using MacVector (v14.5.2).

2.5. Southern blot analysis

Southern blot analysis and probe preparation were performed as previously described (Di Pietro and Roncero, 1998) using a digoxigenin labelling kit (Roche). Hybridising DNA fragments were detected using anti-digoxenin-AP (Roche) and the CDP-Star (Roche) chemiluminescent substrate.

2.6. Generation of phosphoinositide molecular probes

To generate a toolset that enabled a comprehensive microscopic analysis of PIs in filamentous fungi, fluorescent molecular probes specific for various PI species were generated (Table 1). A description of the specific probes used here, support for their lipid specificity as established by previously published *in vitro* lipid binding assays using purified protein, as well as their possible limitations, and an overview of their use *in vivo* to detect specific PI species in mammalian cell lines, plants and fungi, is provided in Methods S2. As mammalian lipid binding domains have been studied in greater detail, each probe was comprised of a characterized mammalian lipid-binding domain specific to one of the respective PIs translationally fused to a C-terminal eGFP or an N-terminal mCherry protein. Codon-optimised constructs were expressed under the control of the *Aspergillus nidulans gpdA* promoter, which drives high level protein expression in *E. festucae* (Hassing et al., 2020), and transformed into *E. festucae* Fl1 protoplasts. Construct integration was verified by PCR and correct expression of the molecular probes was subsequently confirmed by western blot analysis (Fig. S2). Because strain Fl1 produces very few asexual spores, the constructs were also transformed into *E. festucae* strain E2368, a prolific producer of conidiospores (Wilkinson et al., 2000).

2.7. Preparation of constructs

All constructs were designed in MacVector (v14.5.2) and assembled via Gibson assembly (Gibson, 2009). A detailed description of all constructs can be found in Methods S1. All primer sequences and generated plasmids can be found in Table S2.

2.8. Transformation of organisms

E. coli DH5α cells were made chemically competent and transformed as previously described (Hanahan, 1983). *E. festucae* strains were transformed by PEG-mediated protoplast transformation (Young et al., 2005). Protoplasts were generated as previously described (Itoh et al., 1994) and transformed with up to 5 μg of the construct of interest. Following an overnight recovery step on regeneration (RG) medium (Young et al., 2005), protoplasts were overlaid with 0.8% (w/v) RG agar containing hygromycin B or geneticin to a final concentration of 150 μg mL^{-1} or 200 μg mL^{-1}, respectively. The gene knockout of *F. oxysporum* protoplasts was generated as previously described (Corral-Ramos et al., 2015).

2.9. Western blot

E. festucae protein extract (30–50 μg), obtained as previously described (Hassing et al., 2020), was resolved on a 7% or 10% (w/v) SDS acrylamide gel and electrophoretically transferred to nitrocellulose membranes. Membranes were blocked with 2.5% trim milk powder in TBS-T and probed with a primary rabbit anti-GFP antibody (Abcam, Cambridge, UK, ab290, 1:3000 or 1:10000 dilution) or a primary rabbit anti-mCherry antibody (Abcam, ab167453, 1:2000 dilution). A secondary goat anti-rabbit HRP antibody (Abcam, ab6721, 1:10000 dilution) was used for the final antibody incubation, and the blots were developed using Amersham ECL Western blotting solution (GE Healthcare Life Sciences, Malborough, USA).

2.10. qRT-PCR

RNA isolation and qRT-PCR was carried out as previously described using translation elongation factor 2 (*EF-2*) and 40S ribosomal protein S22 (*S22*) as reference genes (Lukito et al., 2015), and primer combinations BH189/BH190 and AC33/AC34 for *tepA* and *mssD*, respectively.

Fungal biomass was quantified using DNA isolated from three biological replicates of pseudostem and blade sections (Liu et al., 2000). Relative biomass was determined by qPCR analysis (SsoFast™ EvaGreen®, Bio-Rad) using the ratio of *pacC* (primers YL113F/YL113R) and *hepA* (primers YL120F/YL120R), single copy endophyte genes (Lukito et al., 2015), to *LpCCR1* (primers YL501F/YL501R and YL502F/YL502R), a single copy plant gene (McInnes et al., 2002). Standard curves were generated by the Lightcycler480® (Roche) software (v1.5.0.) for each primer pair using purified PCR products and absolute quantification qPCR performed with two technical replicates per sample. All primer sequences can be found in Table S2.

2.11. Microscopy

Morphology and growth of cultures, grown on an agar covered glass slide as previously described (Becker et al., 2015), were analysed using an Olympus IX83 inverted fluorescence microscope with the CellSens (version 1.18) software. Imaging was done using the 60× (NA = 1.42) or 100× (NA = 1.4) oil immersion objectives and a QImaging Retiga™ 6000 CCD camera. GFP-fusion protein expressing samples were excited with LED light of 470 nm, mCherry-fusion protein or FM4-48 containing samples with 530 nm and Calcofluor White (CFW) with 380 nm. The emission was collected across the whole spectrum. Cell walls and endomembranes were visualised by staining mycelia with CFW (3 μl of a 3 mg mL^{-1} solution), and FM4-64 (3 μl of a 1.64 μM solution), respectively.

Pseudostem samples were analysed by confocal laser scanning microscopy after labelling with WGA-AlexaFluor 488 (WGA-AF488, Molecular Probes/Invitrogen) and aniline blue diammonium salt (Sigma, St. Louis, USA) (Becker et al., 2016; Becker et al., 2018) using a Leica SP5DM6000B confocal microscope (488 nm argon and 561 nm DPSS

Table 1
Molecular probes generated for this study.

Mammalian protein	Alternative	Accession	Lipid-binding domain	Lipid target	References
Hepatocyte growth factor-regulated tyrosine kinase substrate (HGS)	–	NP_001152800	FYVE (aa 15–222)	PI[3]P	(Burd and Emr, 1998; Gaullier et al., 2000; Gillooly et al., 2000; Vermeer et al., 2006).
Tandem PH-domain-containing protein-2 (TAPP)	Plekha2	NP_112547	PH (aa 195–304)	$PI[3,4]_2$	(Dowler et al., 2000; Kimber et al., 2002).
Mucolipin 1 (TRPML)	–	NP_444407.1	tandem repeat of lipid binding domain (aa 1–68)	$PI[3,5]_2$	(Li et al., 2013).
Bruton's tyrosine kinase (BTK)	–	NP_038510	PH (aa 3–169)	$PI[3,4,5]P_3$	(Rameh et al., 1997; Salim et al., 1996).
Four-phosphate-adaptor protein 1 (FAPP)	Plekha3	NP_112546	PH (aa 1–96)	PI[4]P	(Dowler et al., 2000).
Phospholipase C-δ1 (PLC)		NP_062650	PH (aa 13–139)	$PI[4,5]_2$	(Dowler et al., 2000; Kavran et al., 1998; van Leeuwen et al., 2007; Várnai et al., 2002).

laser, 40 × oil immersion objective, NA = 1.24) (Leica Microsystems) with the LAS AF (version 2.7.3.9723) software.

2.12. Echelon Biosciences Pip3 mass ELISA

Two protocols were trialled for the extraction of phosphoinositides, a protocol provided by Echelon Biosciences with the PIP3 Mass ELISA (K-2500S, Salt Lake City, USA), which is adopted for mammalian cells, as well as a protocol adopted for plant and yeast cells (König et al., 2008). Of the two protocols the second was found to be superior for fungal mycelia as the first, more complex protocol often resulted in the premature split of the organic and aqueous phase. In short, strains of interest were inoculated into PD broth and incubated on a rotary shaker for 5 days. The mycelium was harvested by filtering the culture though a nappy liner to remove the broth. Subsequently the mycelium was dried between stacks of single use hand towels, snap frozen and ground to a fine powder under liquid nitrogen. The powder was weighed (approx. 500 mg) and then added to Corex tubes containing 5 ml of extraction solvent (36% (v/v) CH_3OH, 36% (v/v) $CHCl_3$, 18% (v/v) 2.4 M HCl, and 9% (v/v) 0.4 M EDTA). Following an incubation of 2 h at 4 °C on a rotary shaker the samples were centrifuged to separate the phases and the organic phase was collected. The samples were re-extracted twice with 500 µl of $CHCl_3$ and the combined organic phases were washed twice with 1.5 ml of 0.5 N HCl in 50% (v/v) CH_3OH. The first aqueous phase was discarded and following the second washing step, the organic phase was collected. The organic phases were dried in 10 ml flasks on a Rotovap and stored overnight at −20 °C. The next day each sample was resuspended in 170 µl of the supplied resuspension buffer and vortexed for 4 min. WT samples diluted 1:2 fell below the detection limit of the assay and therefor the results obtained for undiluted samples were used in the calculations described below. Samples were subjected to the ELISA as described in the manufacturer's instructions. The sigmoid standard curve was generated in Microsoft Excel as described previously (dx.https://doi.org/10.17504/protocols.io.78ihrue) and the amount of PI[3,4,5]P_3 in each sample was calculated accordingly. Each amount was divided by the recorded weight of the mycelium resulting in the fmol/mg concentration displayed in the figure. Each WT and mutant strain was analysed three times, of which the first analysis was performed separately from the other two. While all samples were prepared in a random order and treated as similarly as possible, small variations due to the nature of the fungal mycelium used here could not be prevented, possibly explaining the within strain variation in concentration.

2.13. Chemotropism assay

Chemotropic growth of different *F. oxysporum* strains towards tomato root exudate and horseradish peroxidase (HRP; Sigma - Aldrich) was measured using a quantitative plate assay as previously described (Turrà et al., 2015). Microconidia (10^6) embedded in 0.5% water agar, were incubated for 13 h at 22 °C in the presence of a chemoattractant gradient, and the direction of germ tubes relative to a central scoring line was determined using an Olympus binocular microscope at 9200 × magnification. For each sample, five independent batches of cells (n = 100 cells per batch) were scored. The chemotropic index was measured as previously described (Turrà et al., 2015). All experiments were performed at least three times with similar results. Statistical analysis was conducted using the *t*-test for unequal variances, also referred to as Welch's test.

3. Results

3.1. Distribution of phosphoinositides in Epichloë festucae membranes

The localisation of PI[3,4]P_2 and PI[3,4,5]P_3 probes in *E. festucae* hyphae grown in axenic culture or *in planta* was comparable to that of free eGFP and mCherry proteins (Fig. S3). The cytosolic localization of PI[3,4]P_2 probe is consistent with the proposed absence of this lipid species in fungi (De Craene et al., 2017), while the cytosolic localization of the PI[3,4,5]P_3 probe could be due to the absence of this lipid or its presence at a concentration below the detection limit. By contrast, we found that the PI[3]P probe localized to mobile vesicles in conidia and hyphal tips, as well as to the periphery of large oval organelles, presumably vacuoles, present only in mature hyphae (Fig. 1 and Videos S1 & S2). Localization of the PI[3]P probe to endocytic vesicles and the vacuolar membrane was confirmed by co-localization with the membrane marker FM4-64 (Fig. 2A & B). During symbiosis with the plant host, the PI[3]P probes showed a similar distribution to free eGFP or mCherry, localising uniformly throughout the fungal hyphae or in a punctate pattern (Fig. 3). Probes designed for the localization of PI[3,5]P_2 showed a divergent localization pattern in hyphal tips and mature hyphae. While the probe translationally fused to eGFP at the C-terminus localized to vesicle-like structures in hyphal tips and to the periphery of large, oval organelles, presumably vacuoles, in mature hyphae, the probe with the N-terminal mCherry fusion localized to the cytoplasm and within these round organelles (Fig. 1 and Videos S3 & S4). Analysis of the fusion proteins by western blot suggests the mCherry fusion proteins are more susceptible to degradation (Figs. 1 and S2). Both probes occasionally localized to septa (Fig. 1). Co-localization with FM4-64 confirmed the localization of the probe fused to GFP to vacuolar membranes, however, in contrast to the PI[3]P probe, co-localisation to vesicle like structures at the hyphal tip was only rarely observed (Fig. 2C & D). Despite the analysis of multiple infected plants, no fluorescence signal of the PI[3,5]P_2 probe was observed *in planta*, possibly due to weak expression. The PI[4]P probe localized to small mobile vesicles in conidia, hyphal tips and mature hyphae, during growth in axenic culture and *in planta* (Figs. 1 & 3 and Videos S5 & S6). In older hyphae, the cytoplasmic background signal was frequently increased, suggesting a low level or absence of PI[4]P for the probe to bind to or detect, or a higher rate of probe degradation in these senescing hyphae (Fig. 1). Co-localization with Vps52-eGFP, a component of the Golgi-associated retrograde protein complex and a marker protein for late Golgi vesicles (Conibear and Stevens, 2000), confirmed that some of the PI[4]P-containing vesicles were late Golgi vesicles (Fig. 2E & F). Interestingly, the PI[4,5]P_2 probe localized to the periphery and septa of hyphae of all developmental stages, both in culture and *in planta* (Figs. 1 and 3), which was confirmed though co-localization with the chitin-binding dye Calcofluor white (CFW) (Fig. 2G & H). Strikingly, the distribution at the hyphal apex was highly asymmetric, with a reduced signal at the tip and higher fluorescence in the subapical region (Figs. 1 and S4).

3.2. Epichloë festucae encodes a phosphatidylinositol 4-phosphate 5-kinase and a homolog of the mammalian lipid phosphatase and tumour suppressor protein PTEN

We next analysed the role of the lipid kinase, Mss4, and phosphatase, PTEN, the two key enzymes that control the pool of PI[4,5]P_2, the most abundant PI, on hyphal growth and localisation of PI molecular probes in *E. festucae*. The homolog of the *S. cerevisiae* Mss4 phosphatidylinositol 4-phosphate 5-kinase was identified from a tBLASTn analysis of the *E. festucae* Fl1 genome, using the protein sequence of Mss4 (YDR208W) as the query. This search identified a gene (EfM3.031950) encoding a protein of 963 aa (*E*-value 0), hereafter designated as MssD (Fig. 4).

We subsequently identified the *E. festucae* homolog of the mammalian tumour suppressor protein PTEN by performing a tBLASTn analysis against the Fl1 genome using *S. cerevisiae* Tep1 (P53916.1) as a query. This search returned one putative homolog, EfM3.013870, (*E*-value 5e-13), designated as *tepA*, which encodes a predicted protein of 547 aa. Analysis of TepA using InterProScan (Jones et al., 2014) revealed the presence of a dual-specificity phosphatase activity domain (153–202 aa) embedded in the tensin-type phosphatase domain, characteristic of PTEN-type proteins from fungi to humans (Fig. 4). Protein sequence alignment of the tensin-type phosphatase domain of PTEN, *Fg*Tep1,

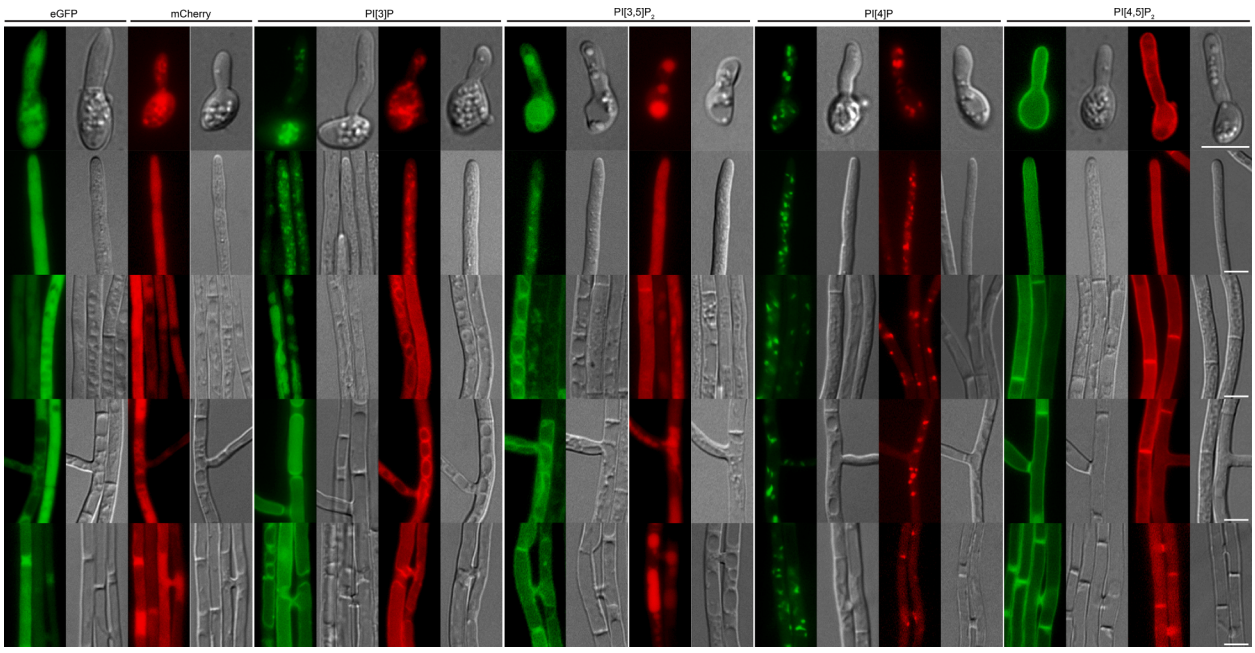

Fig. 1. Localisation of the PI[3]P-, PI[3,5]P_2-, PI[4,]P-, and PI[4,5]P_2- molecular probes in *Epichloë festucae* hyphae grown in axenic culture. Strains were grown on 1.5% H_2O agar for 5 d before examination using an epifluorescence microscope. Images shown are representative of all strains analysed and show localisation of the molecular probes in hyphae of different ages. Images of spores were acquired from transformed *E. festucae* E2368 strains (with the exception of ML1 molecular probes), whereas remaining ones are from transformed Fl1 (with the exception of PI[3,5]P_2 molecular probes). Cytosolic eGFP (pCE25): #T5 (E2368), #T8 (Fl1); cytosolic mCherry (pCE126): #T7 (E2368), #T2 (Fl1), HGS-eGFP (PI[3]P, pCE106): #T7 (E2368), #T9 (Fl1); mCherry-HGS (PI[3]P, pCE111): #T29 (E2368), #T37 (Fl1); ML1-eGFP (PI[3,5]P_2, pBH87): #T5 (spores and axenic culture, Fl1); mCherry-ML1 (PI[3,5]P_2, pBH88): #T12 (spores), #T6 (axenic culture, Fl1); Plekha3-eGFP (PI[4]P, pCE109): #T2 (E2368), #T3 (Fl1); mCherry-Plekha3 (PI[4]P, pCE114): #T16 (E2368), #T25 (Fl1); PLC-eGFP (PI[4,5]P_2, pCE105): #T10 (E2368), #T6 (Fl1); mCherry-PLC (PI[4,5]P_2, pCE110): #T5 (E2368), #T16 (Fl1); Bar = 5 μm.

TepA, *Sp*Ptn1 and *Sc*Tep1 demonstrated an *S. cerevisiae*-specific insertion in *Sc*Tep1, as well as an apparent filamentous fungus-specific insertion in TepA and *Fg*Tep1 (Cid et al., 2008).

Analysis of previously published gene expression data (Chujo et al., 2019; Eaton et al., 2015; Hassing et al., 2019), revealed that *tepA* and *mssD* had intermediate levels of expression in cultures of wild type (20.76 RPKM and 34.57 RPKM, respectively, where RPKM is Reads Per Kilobase of transcript, per Million mapped reads) but no differential expression of either gene *in planta* when wild-type was compared with each of four different symbiotic mutants (Δ*sakA*, Δ*noxA*, Δ*proA*, or Δ*hepA*).

3.3. *Epichloë festucae MssD and TepA exhibit distinct localisation patterns*

Mammalian PTEN has been described to bind to the PM over a very short period (a few hundred milliseconds) to dephosphorylate PI[3,4,5]P_3 before dissociating again to the cytoplasm (Vazquez et al., 2006). By contrast, Mss-4 associates stably with the PM in the subapical region and with cytosolic filaments or endomembranes of an unknown nature in *Neurospora crassa* (Mähs et al., 2012). To analyse the localization of TepA and MssD in *E. festucae,* we generated mCherry and eGFP fusion constructs (Methods S1), transformed into wild-type (WT) protoplasts and verified expression of the complete fusion proteins by western blot (Fig. S5). The eGFP-MssD fusion protein localized to the PM and septa of hyphae of all ages (Fig. 5). Localisation to the PM was irregular and punctate and the fluorescence signal at the hyphal tips was very weak, in contrast to the extended PM localization of the PI[4,5]P_2 molecular probe (Fig. 1). In mature hyphae, the signal was frequently observed in the membrane of small round organelles. For the TepA-mCherry and the eGFP-TepA fusion proteins, slight differences in the localisation were observed. The eGFP-TepA fusion protein localized in the cytoplasm of hyphal tips and young hyphae, similar to constitutively expressed eGFP and mCherry. By contrast, the TepA-mCherry localized to the cytoplasm as well as to septa in hyphae of all ages (Fig. 5).

3.4. *Loss of tepA leads to accumulation of PI[3,4,5]P_3 in hyphal septa*

To test if TepA and MssD affect the concentration and localisation of different PIs, we generated *mssD* and *tepA* deletion and overexpression strains. Gene replacement by homologous recombination yielded three *E. festucae tepA* deletion strains named #T80, #T87 and #T102 (Fig. S6). By contrast, no *mssD* deletion strains were identified after screening ~ 200 transformants, suggesting that *mssD* is essential in *E. festucae*, as previously described in *S. cerevisiae* and *N. crassa* (Mähs et al., 2012; Yoshida et al., 1994).

MssD and TepA overexpression strains were generated by transforming WT protoplasts with plasmids containing the *mssD* (pCE101) or *tepA* (pCE122) gene under the control of the *A. nidulans gpdA* promoter. The transcript levels of *mssD* and *tepA* in a number of transformants were determined by RT-qPCR, and strains that showed increased transcript levels compared to the WT were used for subsequent studies: *mssD* OE: #T17, #T20, #T53 and *tepA* OE: #T4, #T7, #T20 (Fig. S7). Interestingly, all of the *mssD* overexpression (OE) transformants analysed showed relatively low levels of *mssD* overexpression (Fig. S7), suggesting that a high expression level of *mssD* could be detrimental to *E. festucae*.

We then tested whether the overexpression of *mssD* or *tepA*, or the deletion of *tepA* affected the concentration and localisation of different PIs by transforming these constructs into protoplasts of WT, the *tepA* deletion strains #T87 and #T102, the *tepA* overexpression strain #T7 and the *mssD* overexpression strain #T17, which showed the highest levels of expression in culture. Using the PI[4,5]P_2 or the PI[3,4,5]P_3 molecular probes, a signal pattern similar to that of WT hyphae was observed in the different mutant strains (Figs. 1 and 6). However, the Δ*tepA* mutants showed an accumulation of PI[3,4,5]P_3 at septa in

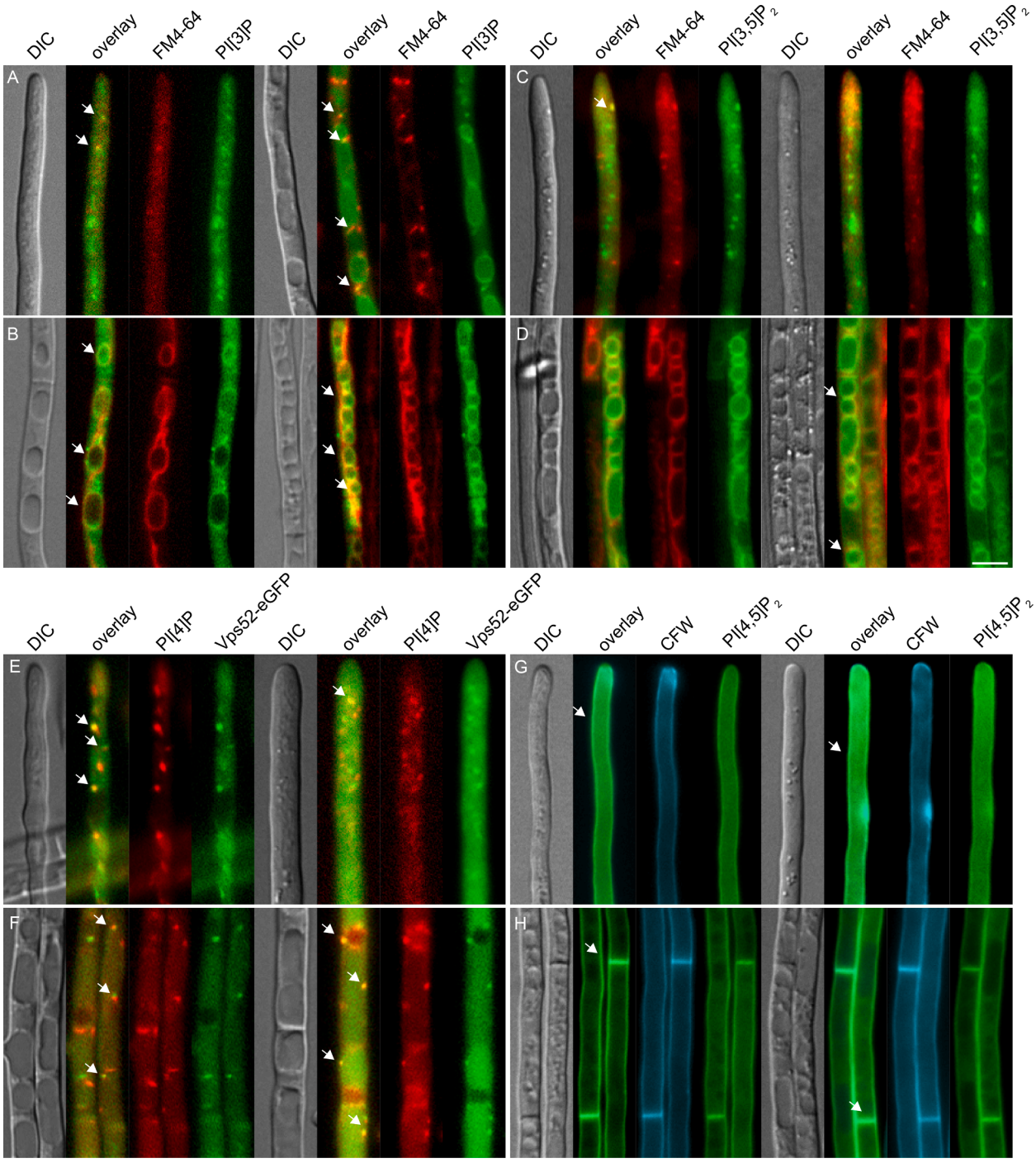

Fig. 2. Co-Localisation with compartment-specific fluorescent markers of the PI[3]P- and PI[4]P- molecular probes in *Epichloë festucae* hyphae grown in axenic culture. Strains were grown on 1.5% H_2O agar for 5 d before examination using a fluorescence microscope. Images shown are representative of all strains analysed and show localisation of the molecular probes in hyphae of different ages. (A and B) Co-localisation of the PI[3]P molecular probe with the membrane marker FM4-64. In (A) FM4-64 was added and cultures were analysed immediately to observe endocytic vesicles, while in (B) the stain was added and the cultures were incubated 16 h before analysis, resulting in the staining of vacuolar membranes. Images shown are from the strains HGS-eGFP (PI[3]P, pCE106) #T9 and #T24. (C and D) Co-localisation of the PI[3,5]P_2 molecular probe with the membrane marker FM4-64. In (C) FM4-64 was added and cultures were analysed immediately to observe endocytic vesicles, while in (D) the stain was added and the cultures were incubated 1 h before analysis, resulting in the staining of vacuolar membranes. Images shown are from the strains ML1-eGFP (PI[3,5]P_2, pBH87) #T5. (E and F) Co-localisation of the PI[4]P- molecular probe with Vps52-eGFP (pKG55), a marker protein for late Golgi vesicles (Conibear and Stevens, 2000). In (E) hyphal tips are shown, where co-localisation was frequently difficult to observe due to cytoplasmic movement, while (F) shows more mature hyphae. Images are from the strain mCherry-Plekha3 (PI[4]P, pCE114) #T25 transformed with the plasmid pKG55 (Vps52-eGFP) resulting in the strains #T35 and #T43. (G and H) Co-localisation of the PI[4,5]P_2 molecular probe with the chitin stain Calcoflour white. In (g) hyphal tips are shown, while (h) shows more mature hyphae. Images shown are from the strains PLC-eGFP (PI[4,5]P_2, pCE105) #T6. White arrows show areas of co-localisation. Bar = 5 μm.

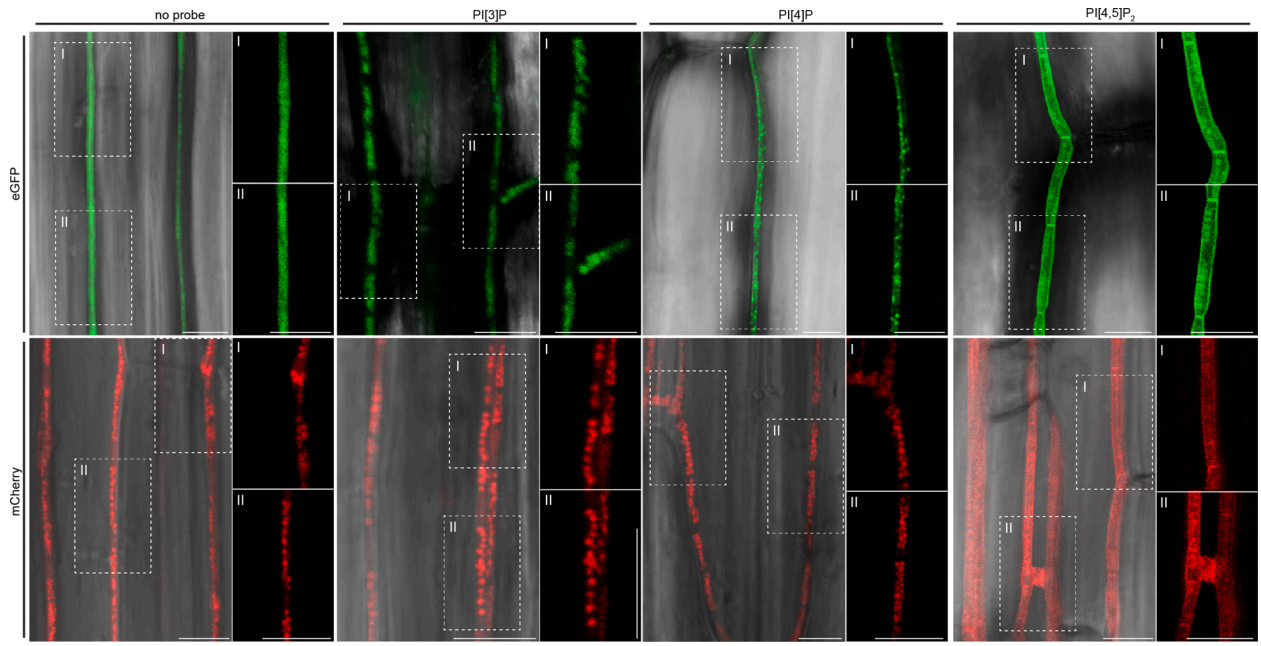

Fig. 3. Localisation of the PI[3]P-, PI[4]P- and PI[4,5]P_2- molecular probes in *Epichloë festucae* during interaction with *Lolium perenne*. Confocal laser scanning microscopy images of *E. festucae* strains constitutively expressing eGFP, mCherry or the PI molecular probes *in symbio* with *L. perenne*. Samples were freshly harvested from the innermost layer of the pseudostem at 9–14 weeks post-inoculation and mounted in deionised water for analysis. Images labeled with (I) or (II) show enlarged images of the region indicated in the neighbouring image. Cytosolic eGFP (pCE25): #T8; cytosolic mCherry (pCE126): #T2; HGS-eGFP (PI[3]P, pCE106): #T9; mCherry-HGS (PI[3]P, pCE111): #T37; Plekha3-eGFP (PI[4]P, pCE109): #T3; mCherry-Plekha3 (PI[4]P, pCE114): #T25; PLC-eGFP (PI[4,5]P_2, pCE105): #T6; mCherry-PLC (PI[4,5]P_2, pCE110): #T10; Bar = 10 μm.

hyphae of all ages (Fig. 6), supporting the hypothesis that *E. festucae* TepA is a functional phosphatidylinositol 3,4,5-trisphosphate 3-phosphatase.

To collect further evidence in support of this hypothesis, the concentration of PI[3,4,5]P_3 in WT and mutant fungal mycelium was measured, using a PI[3,4,5]P_3 enzyme-linked immunosorbent assay (ELISA, Echelon) frequently used with mammalian cells. We found that the concentration of PI[3,4,5]P_3 in the three independent *tepA* deletion mutants was consistently higher than in WT (Fig. 7, Fig. S8). In the *tepA* deletion strains #T80 and #T87 we detected a 5.4- and 5.8- fold increase in PI[3,4,5]P_3 concentration compared to WT, values close to the 6–8 fold increased concentration in the *S. pombe* Ptn1 deletion strain (Mitra et al., 2004). However, because of the variation within biological replicates, especially in the *tepA* deletion strain #T102, only differences between WT and the deletion strain #T87 were significant ($p = 0.007$) (Figs. 7 & S8).

3.5. Overexpression of Epichloë festucae mssD or tepA, or deletion of tepA does not affect hyphal growth in culture or in planta

To analyse the role of MssD and TepA in *E. festucae*, growth of WT and mutant strains were compared in axenic culture. The growth rate and morphology of the *mssD* overexpression strains and the *tepA* deletion and overexpression strains were indistinguishable from the WT (Fig. S9). Similar to the WT, these strains showed smooth hyphae of a uniform diameter, formation of hyphal bundles, hyphal coils and hyphal cell-to-cell fusions (Fig. S9). Cell wall staining of WT and mutant hyphae with CFW resulted in a similar even pattern of fluorescence (Fig. S9). We conclude that overexpression of *mssD* or *tepA*, or deletion of *tepA* have no detectable effect on the growth of *E. festucae* in axenic culture.

In previous studies, deletion of the PTEN homologs in *F. graminearum* and *U. maydis* resulted in a decrease in virulence on wheat and maize, respectively (Vijayakrishnapillai et al., 2018; Zhang et al., 2010). Here we found that *L. perenne* plants infected with the *tepA* deletion mutant of *E. festucae* and scored 10 weeks post-inoculation, were not consistently significantly different from WT-infected plants in leaf length and tiller number (Fig. 8B and S10). Similar results were observed for plants infected with the *tepA* overexpression strains (Fig. 8C and S10). Interestingly, plants infected with *mssD* overexpression strains #T20 and #T53 had significantly longer tillers than those infected with the WT (Fig. 8A and S10). This phenotype was previously correlated with a decreased fungal biomass *in* planta (Kayano et al., 2018). We therefore measured the fungal biomass in plants using qPCR and found that the fungal biomass was significantly reduced in plants infected with the *mssD* overexpression strain #T20 and reduced (but not significant) in plants infected with the overexpression strain #T53 (Fig. S11), supporting the conclusion that the longer tiller phenotype correlates with reduced fungal colonization as previously observed (Kayano et al., 2018).

To visualize fungal hyphae in the plant tissue, longitudinal sections of the pseudostem of infected plants were infiltrated with the chitin-specific probe WGA-AF488 and the β-glucan-binding dye aniline blue. The growth pattern of the different mutant strains was similar to that of the WT, showing one or two hyphae between neighbouring plant cells, which branch and fuse with neighbouring hyphae to give rise to a hyphal network throughout the plant (Fig. S12).

3.6. Fusarium oxysporum TepA is required for chemotropic hyphal growth towards tomato roots

Previously PI[3,4,5]P_3 signaling was shown to be required for cell polarity and chemotaxis in mammalian cells and in the slime mould, *Dictyostelium* (Balla, 2013; Heit et al., 2008; Iijima and Devreotes, 2002; Iijima et al., 2004; Weiger and Parent, 2012). While chemotaxis has not been studied in *E. festucae* to date, the fungal pathogen *F. oxysporum* has been established as a model system to study fungal chemotropism, demonstrating that hyphae are chemotropically attracted to tomato roots by secreted plant peroxidases (Turrà et al., 2015). Here we tested the role of TepA in chemotropism of *F. oxysporum* by generating targeted deletion mutants in the *tepA* ortholog *FOXG_09154*. Southern blot

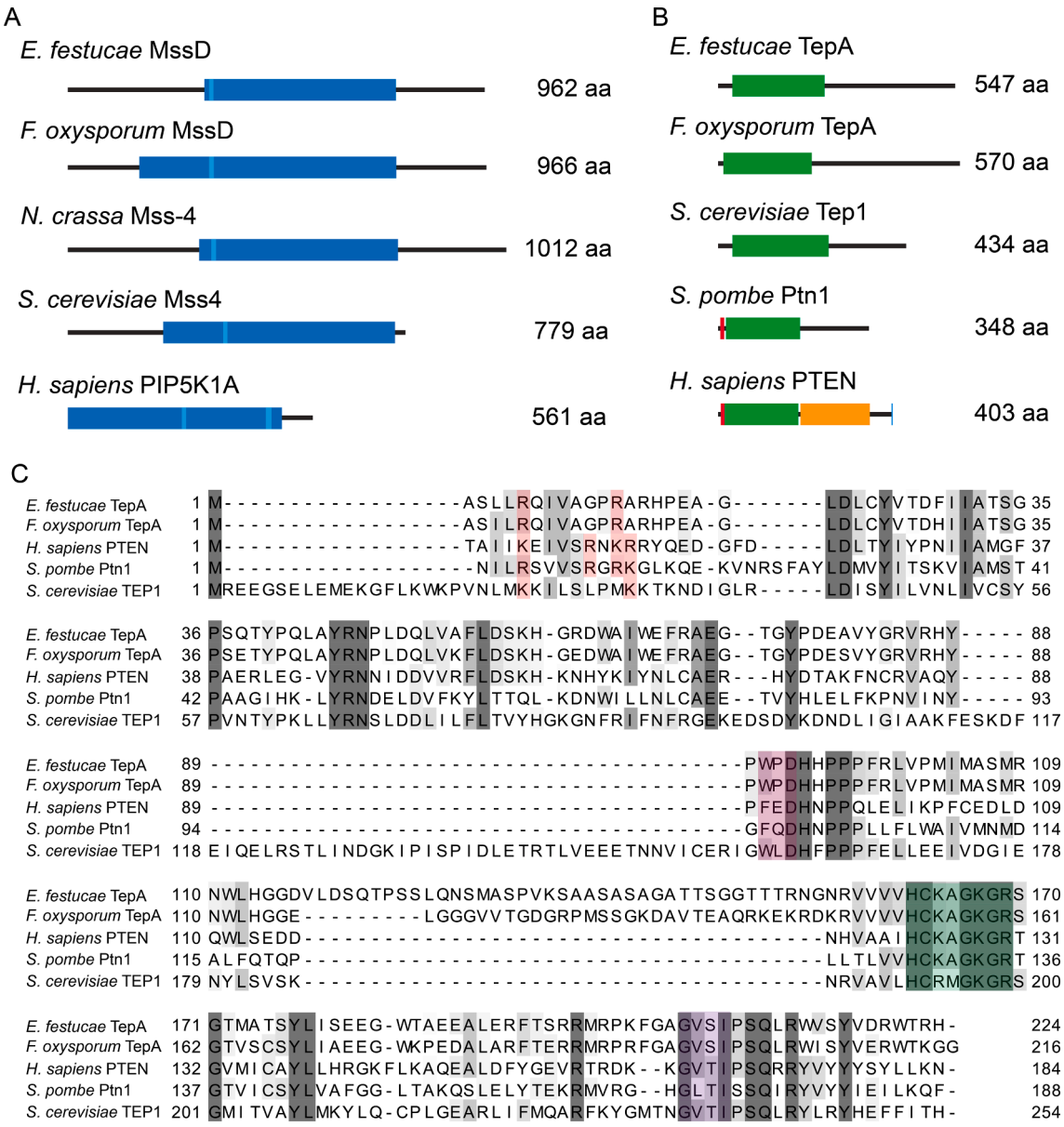

Fig. 4. Domain structure of *Epichloë festucae* MssD and TepA, and comparison to homologs from other fungi and humans. (A) Schematic representation of *E. festucae* MssD, *F. oxysporum* MssD (XP_018251113.1), *N. crassa* Mss-4 (NCU02295), *S. cerevisiae* Mss4 (YDR208W), and human PIK5P1A (Q99755). Dark blue box: phosphatidylinositol-4-phosphate 5-kinase domain (IPR023610), light blue box: Nuclear localisation signal (cNLS Mapper, (Kosugi et al., 2008; Kosugi et al., 2009a; Kosugi et al., 2009b)), human PIK5P1A contains a bipartite NLS. Size of the protein indicated in number of aa. (B) Schematic representation of *E. festucae* TepA, *Schizosaccharomyces pombe* Ptn1 (CAA22831.1), *Saccharomyces cerevisiae* Tep1 (P53916.1), *Fusarium oxysporum* TepA (XP_018246213.1) and *Homo sapiens* PTEN (AAD13528.1). Green box: tensin-type phosphatase domain, red box: PI[4,5]P_2-binding domain, orange box: C2 domain, blue box: PDZ binding motif. Size of the protein indicated in number of aa. (C) Amino acid sequence alignment of the tensin-type phosphatase domain of TepA, *Sp*Ptn1, *Sc*TEP1, *Fo*TepA and *Hs*PTEN; red highlights: conserved aa of the PI[4,5]P_2-binding domain; light purple box: WPD-loop; green box: P-loop (active site); dark purple box: Ti-loop. Sequences were annotated according to InterProScan (Jones et al., 2014) and by comparison of the domains identified by (Lee et al., 1999). Sequences are shaded in a grey scale based on their percentage identity.

analysis identified a number of transformants in which the wild-type gene had been replaced with the null allele (Fig. S13). Colony growth and conidiation of these mutants was indistinguishable from the WT (Fig. S14). Moreover, the mutants did not significantly differ from the WT in causing mortality in tomato plants in a root inoculation assay (Fig. S15). These results suggest that TepA is not required for hyphal growth, development and virulence of *F. oxysporum*.

Next, we investigated the role of TepA in chemotropism and found that the *tepA* deletion mutants were fully impaired in directional growth towards tomato root exudate and commercial horseradish peroxidase (Fig. 9). This suggests that PI[3,4,5]P_3 signaling is required for hyphal chemotropism of *F. oxysporum* towards plant roots.

4. Discussion

Phosphoinositides (PI) have been implicated in many key cellular processes including cytoskeleton rearrangement, establishment of cell polarity, regulation of ion channels and the control of cellular proliferation and cancer (De Craene et al., 2017). In this study, we provide evidence for the localisation of the PI species PI[3]P, PI[3,5]P_2, PI[4]P and PI[4,5]P_2 in a filamentous ascomycete, and show that this species is able to produce PI[3,4,5]P_3. While we found that the homologs of the

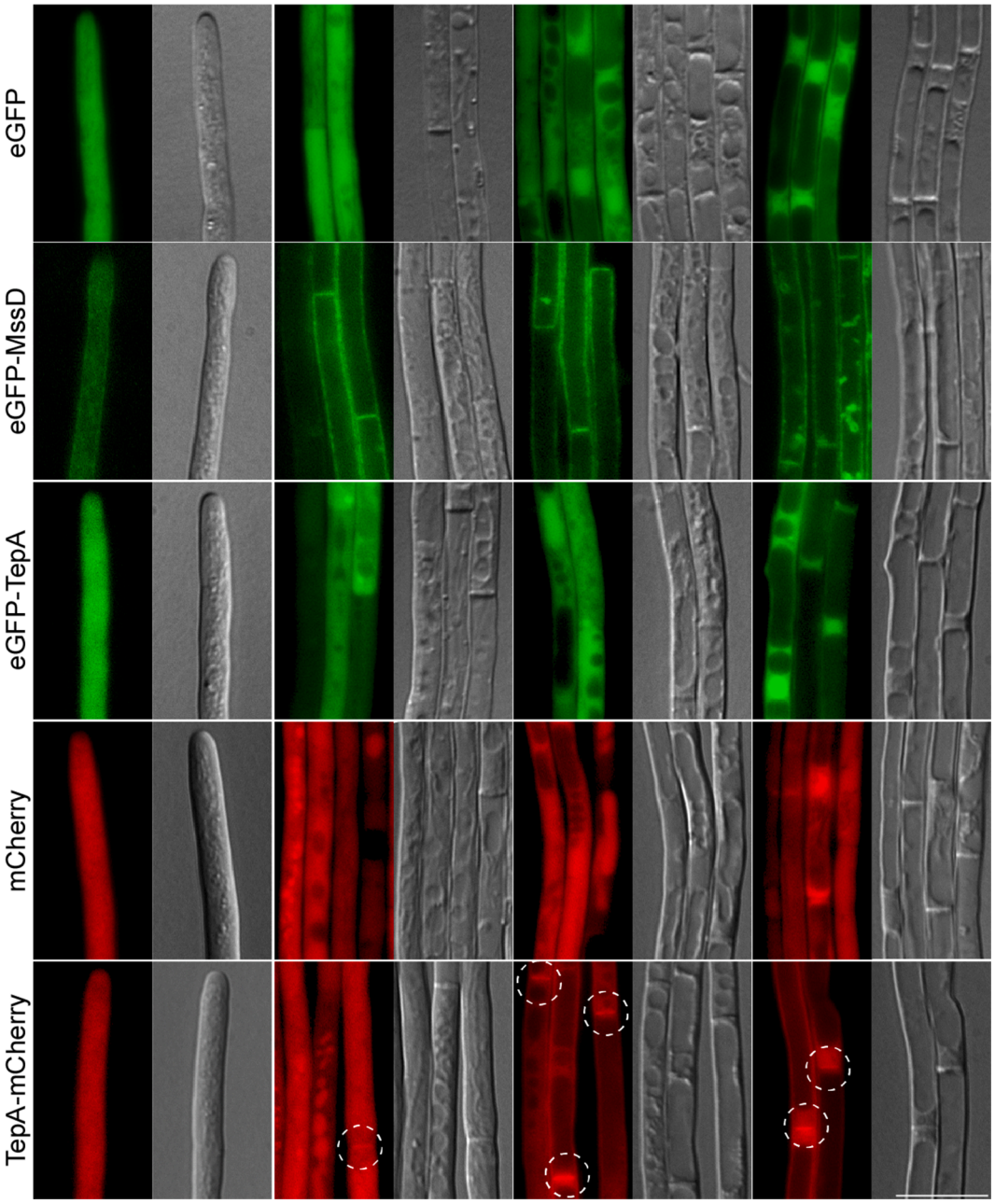

Fig 5. Localisation of TepA and MssD during axenic growth of *Epichloë festucae*. Strains were grown on 1.5% H_2O agar for 5 d before examination using a epi-fluorescence microscope. The images shown of wild-type (WT) expressing eGFP (pBH28, #T6), eGFP-MssD (#T8), eGFP-TepA (pBH41, #T4), mCherry (pCE126, #T2) and TepA-mCherry (pBH42, #T2) are representative of all strains analysed. As indicated, hyphae of different ages were analysed. White circles: localisation of the fusion protein at septa. Bar = 10 μm.

mammalian PTEN protein are not required in the mutualistic interaction between *E. festucae* and *L. perenne* and the pathogenic interaction between *F. oxysporum* and tomato, we identified PTEN to be essential for the ability of a fungus to undergo chemotrophic hyphal growth towards plant roots.

The molecular probe for PI[3]P (Vermeer et al., 2006) displayed two distinct localization patterns in cells of axenic cultures: vesicle-like structures, some of which are endocytic vesicles, and the periphery of vacuoles. Similar observations were made in mammalian and yeast cells, where PI[3]P was identified in early endosomes and in internal vesicles of both multivesicular endosomes and vacuoles (Gillooly et al., 2000; Marat and Haucke, 2016), fulfilling key roles in membrane trafficking and vesicle fusion throughout the endosomal system (Balla, 2013; Marat and Haucke, 2016).

The PI[3,5]P_2 probe (Li et al., 2013) fused to eGFP at the C-terminus localized to vacuolar membranes in mature hyphae and septa, and to mobile vesicles in hyphal tips. PI[3,5]P_2 is generated and regulated by a vacuolar membrane protein complex in yeast and mammals, and localizes to the vacuolar/lysosomal membranes and endosomes, where it is involved in late endosomal protein sorting and autophagy (De Craene et al., 2017; McCartney et al., 2014). Interestingly, the vesicle like structures observed in hyphal tips did not appear to be endosomal vesicles and therefore the nature of these vesicles remains to be identified. While the specificity of several of the other lipid binding domains used here have been extensively studied and used for over a decade, the ML1 tandem domain has only been used relatively recently so its specificity is less well established. Nonetheless the probe has been used in multiple studies in mammalian cells (Ariotti et al., 2015; Barklis et al., 2018; Li

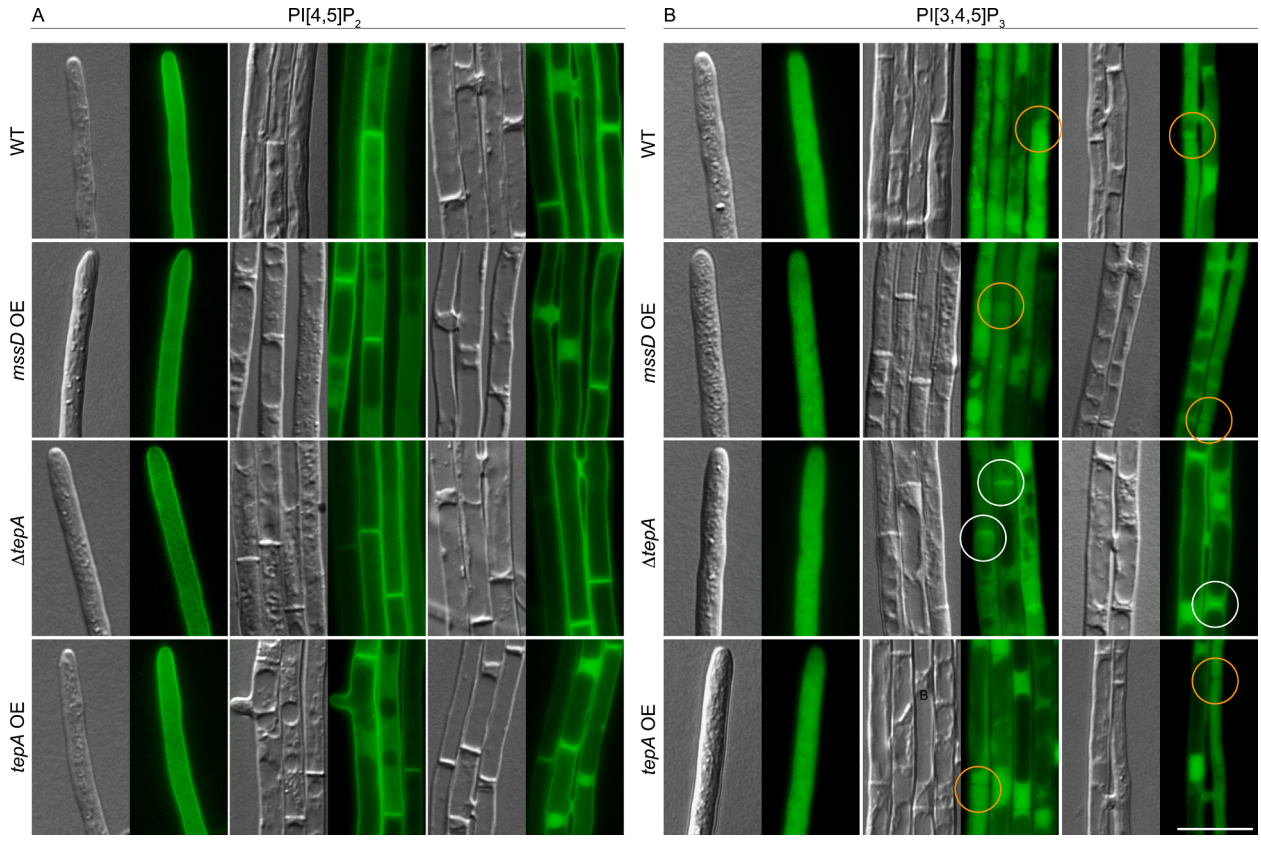

Fig. 6. Localisation of PI[4,5]P_2 and PI[3,4,5]P_3 in *Epichloë festucae* wild-type, *tepA* and *mssD* mutant strains. The indicated strains were incubated on 1.5% H_2O agar for approx. 5 d before analysis by fluorescence microscopy. eGFP-based Molecular probe constructs were transformed into WT, the *tepA* deletion strain #T87, the *tepA* overexpression strain #T7 and the *mssD* overexpression strain #T17. Multiple transformants were analysed and images shown are representative of all transformants analysed. (A) Localisation of the PI[4,5]P_2 molecular probe (pCE107) in WT (#T3), *mssD* overexpression (#T8), *tepA* overexpression (#T6) and *tepA* deletion (#TN2) strains. (B) Localisation of the PI[3,4,5]P_3 molecular probe (pCE105) in WT (#T9), *mssD* overexpression (#T8), *tepA* overexpression (#T1) and *tepA* deletion (#T15) strains. White circles: localisation of the molecular probe at septa. Orange circles: No localisation of the molecular probe at septa. Bar = 10 μm.

et al., 2013) and no alternative probe has yet been suggested (Hasegawa et al., 2017).

The molecular probe for PI[4]P (Vermeer et al., 2009) localized to highly mobile vesicle-like structures throughout hyphae in culture and *in planta*, some of which were Golgi-derived vesicles as confirmed by co-localization with Vps52, a marker for late Golgi vesicles (Conibear and Stevens, 2000). Although this probe has been shown to also bind Arf1 (Godi et al., 2004), deletion of the gene encoding this protein in *C. albicans* did not affect the punctate Golgi-specific localization observed in wild-type (Ghugtyal et al., 2015). In yeast and mammals, PI[4]P localizes in two distinct pools, at the Golgi and the PM, which are maintained through the presence of different PI4Ks (De Craene et al., 2017; De Matteis et al., 2013). In yeast, Golgi localized PI[4]P is crucial for vesicle formation in anterograde and retrograde transport, while the PM pool is required for targeting specific proteins to the PM, resulting in distinct functions in actin cytoskeleton organization, cell wall integrity, and receptor-mediated endocytosis (Audhya and Emr, 2003; Audhya et al., 2000; Baird et al., 2008; Ghugtyal et al., 2015; Hammond et al., 2012; Yamamoto et al., 2018). However, no PM localization of the PI[4]P molecular probe was observed in *E. festucae* hyphae.

The PI[4,5]P_2 molecular probe (van Leeuwen et al., 2007) localized to the PM and septa of *E. festucae* hyphae in axenic culture and *in planta*. Indeed, PI[4,5]P_2 is the major phosphoinositide at the inner leaflet of the PM across kingdoms, where it serves as a precursor for other signaling molecules and fulfils roles in cell polarity, endo- and exocytosis, actin cytoskeleton rearrangement and activation of transporters (De Craene et al., 2017; Di Paolo and De Camilli, 2006). Strikingly, the PI[4,5]P_2 molecular probe had an asymmetric localisation in vegetatively growing hyphal tips, where there was little signal at the hyphal apex, but a strong signal in the sub-apical region. An asymmetric distribution of PI[4,5]P_2 at sites of polar growth has been observed in many organisms including tobacco pollen tubes and in *N. crassa*, and is required for the yeast to hyphal transition of *Candida albicans* (Ischebeck et al., 2008; Mähs et al., 2012; Vernay et al., 2012). In contrast to this study, the fluorescent signal for PI[4,5]P_2 in *C. albicans, S. cerevisiae and N. crassa* was strongest at the hyphal apex (Guillas et al., 2013; Mähs et al., 2012; Vernay et al., 2012). Interestingly, the subapical concentration of this molecular probe coincided with the so-called endocytic collar, a region with increased endocytic activity (Echauri-Espinosa et al., 2012; Taheri-Talesh et al., 2008).

While MssD and its fungal homologs are relatively conserved with the mammalian phosphatidylinositol-4-phosphate 5-kinase, the *E. festucae* TepA shows differences to human PTEN regarding different lipid binding motifs (Lee et al., 1999; Nguyen et al., 2014; Vazquez et al., 2006; Walker et al., 2004). Therefore, differences in the ability of the *E. festucae* protein to bind, and to be recruited, to membranes are likely. Indeed, in mammalian cells, PTEN was found to localize to the cytosol, membranes, nuclei, mitochondria and ER (Bononi et al., 2013; Bononi and Pinton, 2015; Putz et al., 2012; Zhu et al., 2009), which was not observed for *E. festucae* TepA. Instead TepA localized to the cytosol as well as to septa of hyphae grown in axenic culture, a result similar to what has been observed for the PTEN homolog in *S. pombe* (Mitra et al., 2004).

Unlike TepA, MssD localized to the PM in a punctate pattern, with the signal being weak at the hyphal tip and increasingly stronger in older hyphae. In contrast, in *N. crassa*, Mss-4 localized to the membrane only

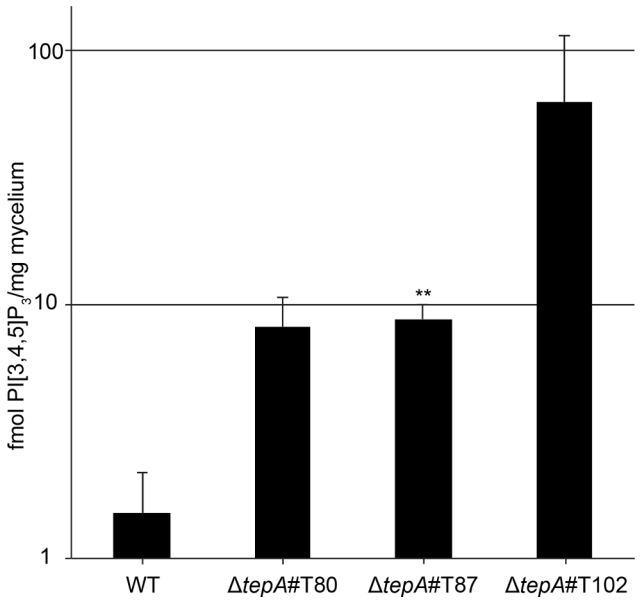

Fig. 7. Deletion of in *Epichloë festucae tepA* results in an accumulation of PI[3,4,5]P_3 in *tepA* mutant strains compared to the wild-type. WT and *tepA* mutant strains were prepared as described and the ELISA was conducted as outlined in the manufacturer's description. Each strain was analysed in three biological replicates. The first repetition was conducted separately from the following two. *p*-values were calculated by a two-tailed Student *t*-Test and asterisks represent statistically significant differences in the PI[3,4,5]P_3 concentration of *tepA* deletion mutants (*$p \leq 0.05$; **, $p \leq 0.01$; ***, $p \leq 0.001$) compared to the WT. WT vs. *tepA* deletion strain #T80 $p = 0.058$; WT vs. *tepA* deletion strain #T87 $p = 0.007$; WT vs. *tepA* deletion strain #T102 $p = 0.305$.

subapical to the hyphal tip and at septa, as well as to non-defined intracellular filamentous structures (Mähs et al., 2012).. while *S. cerevisiae* Mss4 was found to localize evenly at the PM. This indicates that localisation of Mss4 may not be universally conserved (Audhya and Emr, 2003; Homma et al., 1998; Vernay et al., 2012). Interestingly, the localisation of eGFP-MssD correlated with the localization of the PI[4,5]P_2 molecular probe in mature hyphae of *E. festucae*, but not at the hyphal tip.

Attempts to delete *E. festucae mssD* were unsuccessful, indicating that it is essential for fungal growth, as has been observed in *N. crassa* and in yeast (Desrivières et al., 1998; Mähs et al., 2012). Conditional mutants have demonstrated essential roles for Mss-4 in actin organization, hyphal morphogenesis and yeast to filamentous growth transition in *C. albicans* (Homma et al., 1998; Mähs et al., 2012; Vernay et al., 2012). Overexpression of *mssD* in *E. festucae* did not change the hyphal morphology in axenic culture, but the highest expression level obtained was approx. 6-fold relative to the WT *mssD* expression, which is low compared to the level of overexpression achieved with the same promoter for *tepA* (approx. 200 fold) or other proteins (Hassing et al., 2020). Thus, it is possible that overexpression of *mssD* negatively impacts on fungal growth.

Both *E. festucae tepA* deletion and overexpression strains and *tepA* deletion mutants of *F. oxysporum* were indistinguishable from WT in their hyphal growth rate and colony morphology, a result similar to what has been observed for deletion of this gene in *F. graminearum* and *U. maydis* (Vijayakrishnapillai et al., 2018; Zhang et al., 2010).

Inoculation of the *E. festucae tepA* deletion mutants into *L. perenne* did not significantly change growth of the host plant when compared to a WT interaction. Similarly, *F. oxysporum* Δ*tepA* strains were equally virulent on tomato plants as WT. Interestingly, the corresponding TepA homologs in *F. graminearum* and *U. maydis* have been shown to be required for virulence on wheat and maize, respectively (Vijayakrishnapillai et al., 2018; Zhang et al., 2010). These species differences might be the result of slightly different infection processes, such as a requirement for chemotaxis.

Interestingly, leaves of *L. perenne* plants infected by two *mssD* overexpression strains were significantly longer than those of WT-infected plants which correlated with reduction in fungal biomass in plants infected with these two strains. A similar phenotype has previously been described for the *E. festucae cdc42* deletion mutant, where the increased length and reduced fungal biomass was due to defects in intercalary growth (Kayano et al., 2018).

Overexpression of *mssD* and deletion or overexpression of *tepA* did not appear to affect the localisation and concentration of the molecular probe for PI[4,5]P_2.

However, while the molecular probe for the detection of PI[3,4,5]P_3 localized to the cytosol in *mssD* and *tepA* OE strains, in the *tepA* deletion strains it localized to septa, consistent with the localization of TepA fused with mCherry to septa. These results demonstrate that filamentous fungi produce PI[3,4,5]P_3 during normal growth and when combined with the ELISA analysis showing that PI[3,4,5]P_3 accumulates in the *tepA* deletion mutants, suggests that TepA is a functional PI[3,4,5]P_3 phosphatase. Interestingly, the PI[3,4,5]P_3 concentration detected in WT was frequently close to the detection limit of the assay, supporting the hypothesis that the PI[3,4,5]P_3 probe did not show a specific localization pattern in WT due to a low abundance of the lipid species. This low abundance may also account for the high variability observed in the ELISA assay.

As fungi lack homologs of the 3-kinase responsible for the phosphorylation of PI[4,5]P_2, a pathway for the generation of PI[3,4,5]P_3 similar to that described in *S. pombe* seems likely, where the production of this lipid species relies on the class III phosphatidylinositol 3-kinase, Vps34p, and the phosphatidylinositol 4-phosphate 5-kinase, Its3p (Balla, 2013; Mitra et al., 2004).

In the slime mould *Dictyostelium*, cells display a steep PI[3,4,5]P_3 gradient, with highest concentrations of PI[3,4,5]P_3 at the leading edge. Deletion of either the phosphoinositide 3-kinases or PTEN dissipated the PI[3,4,5]P_3 gradient and reduced the efficiency of chemotaxis (Iijima and Devreotes, 2002; Iijima et al., 2004). Chemotaxis in mammalian neutrophils and macrophages also requires a PI[3,4,5]P_3 gradient, although it appears to be regulated in a PTEN-independent way (Weiger and Parent, 2012). Here we found that chemotropism of *F. oxysporum* towards either tomato root exudate or the chemoattractant horseradish peroxidase was impaired in *tepA* deletion mutants, uncovering for the first time a role for PI[3,4,5]P_3 signaling in the control of directional hyphal growth. Moreover, our findings suggest that the role of PI[3,4,5]P_3 in chemosensing is conserved across kingdoms. However, the exact functional link between PI[3,4,5]P_3 and the downstream signaling components regulating chemotropic growth in *F. oxysporum*, such as the CWI MAPK cascade (Turrà et al., 2015), remains to be established. Likewise, it is currently unknown whether an asymmetric distribution of PI[3,4,5]P_3 could govern chemotropism in this fungal pathogen, as described for *Dictyostelium* (Iijima and Devreotes, 2002; Iijima et al., 2004).

In summary, by analysing the localisation of PI species in the fungal endophyte *E. festucae,* we observed distinct localisation patterns for PI[3]P, PI[4]P, PI[3,5]P_2 and PI[4,5]P_2, and identified PI[3,4,5]P_3, a PI species not previously reported in filamentous fungi, which is dephosphorylated by the *E. festucae* PTEN homolog. While deletion of the homologs of PTEN in *E. festucae* and *F. oxysporum* had no impact on the ability of these fungi to form mutualistic or pathogenic interactions with the plant hosts, we show that PTEN homologs are required for fungal chemotropism.

Funding

This research was supported by grants from the Tertiary Education Commission to the Bio-Protection Research Centre, the Royal Society of New Zealand Marsden Fund (MAU1301) and by Massey University.

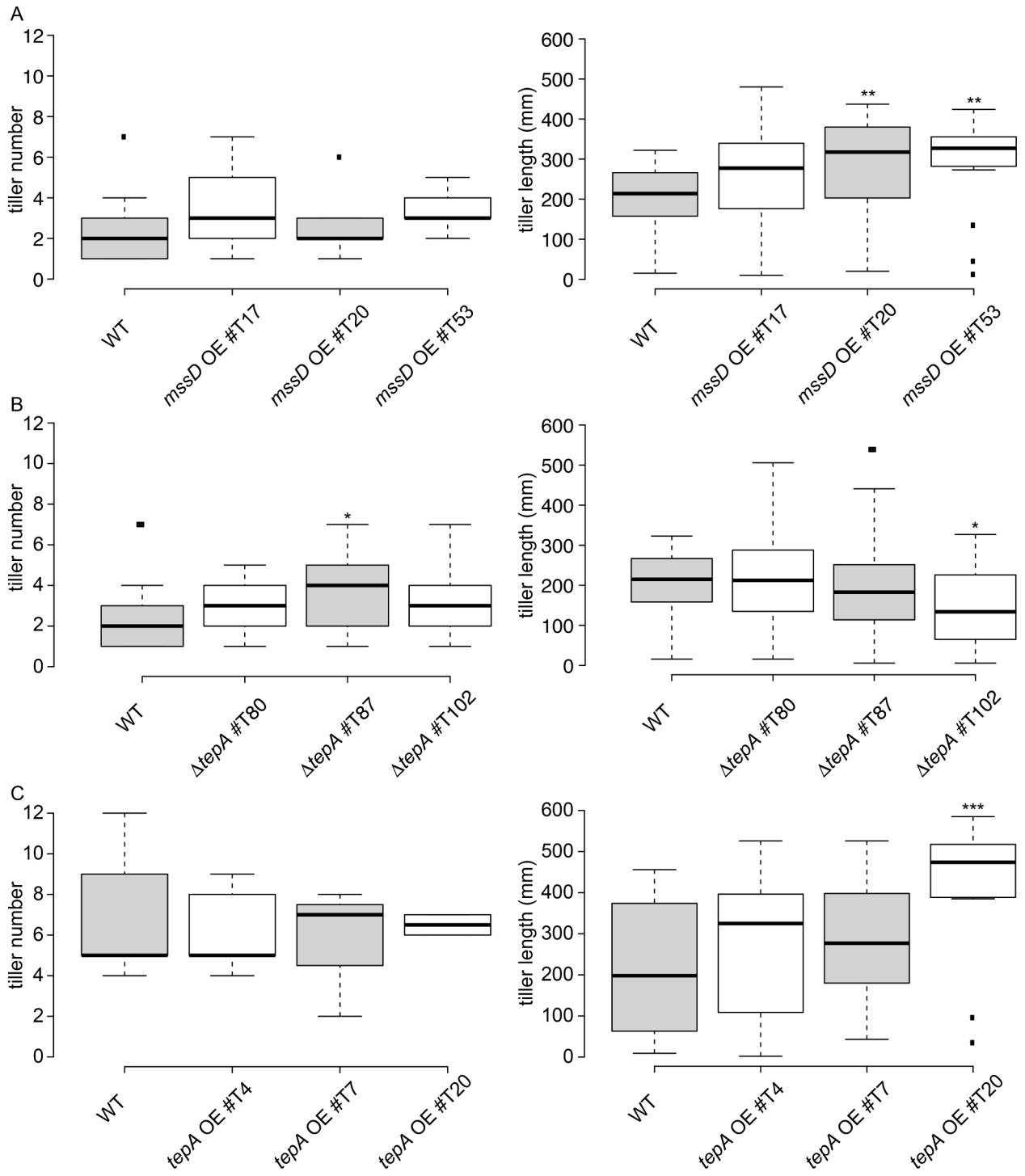

Fig. 8. Growth analysis of *Lolium perenne* plants infected with *Epichloë festucae* wild-type and *tepA* overexpression strains. Tiller number of infected plants: wild-type (WT) (23), *mssD* overexpression strains #T17, #T20, #T53 (n = 18/15/6)(A), *tepA* deletion strains #T80, #T87, #T102 (n = 31/32/18)(B), WT (5), *tepA* overexpression strains #T4, #T7, #T20 (n = 5/3/2)(C). Box plots were generated using BoxPlotR (available on http://shiny.chemgrid.org/boxplotr/). One-way ANOVAs were used to test for differences in plant phenotypes between WT and mutant strains. In each case, the ANOVA was fitted with R and a Bonferroni correction was applied to all *p*-values to account for multiple testing: $*p \leq 0.05$; $**p \leq 0.01$; $***p \leq 0.001$. All other differences are not significant. The highly significant difference regarding the tiller length of the *tepA* OE strain #T20 has not been mentioned in the main text due to the low and therefore statistically insignificant number of biological replicates. Boxes indicate outliers.

Work in the Di Pietro lab was supported by by grants BIO2016-78923-R and PID2019-108045RB-I00 from the Spanish Ministerio de Ciencia e Innovación (MICINN).

CRediT authorship contribution statement

Berit Hassing: Conceptualization, Methodology, Investigation, Validation, Formal analysis, Writing – original draft. **Alyesha Candy:** Investigation, Validation, Formal analysis. **Carla J. Eaton:** Conceptualization, Resources, Supervision, Formal analysis, Project

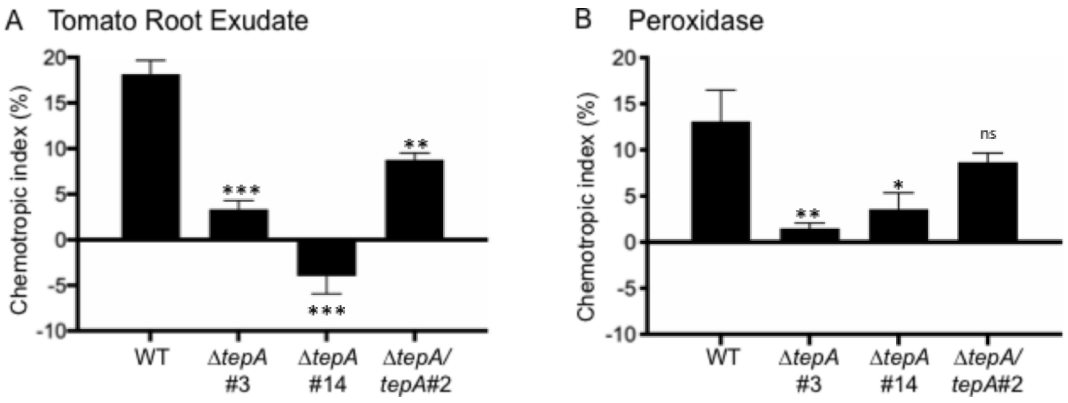

Fig. 9. *Fusarium oxysporum* TepA is required for hyphal chemotropism towards tomato roots. Microconidia of the *F. oxysporum* wild type strain, two knockout mutants and a complemented strain were embedded in water agar and incubated 13 h at room temperature in the presence of a gradient of tomato root exudate (A) or 4 μM horseradish peroxidase (HRP) (B). The direction of germ tubes relative to a central scoring line was determined in an Olympus binocular microscope. Calculation of chemotropic index was done as described (Turrà et al., 2015). $*p \leq 0.05$; $**p \leq 0.01$; $***p \leq 0.001$, *versus* wild-type (WT) strain. Data presented are the mean from at least three independent experiments. n = 500 germ per experiment. Error bars, SD.

administration, Funding acquisition. **Tania R. Fernandes:** Methodology, Investigation, Validation, Formal analysis, Writing – review & editing. **Carl H. Mesarich:** Formal analysis, Supervision, Writing – review & editing. **Antonio Di Pietro:** Conceptualization, Resources, Supervision, Formal analysis, Writing – original draft, Project administration, Funding acquisition. **Barry Scott:** Conceptualization, Resources, Supervision, Formal analysis, Writing – original draft, Project administration, Funding acquisition.

Declaration of Competing Interest

The authors declare that they have no known competing financial interests or personal relationships that could have appeared to influence the work reported in this paper.

Acknowledgements

The authors thank Niki Murray, Pani Vijayan and Matthew Savoian (Manawatu Microscopy and Imaging Centre) for support with microscopy and imaging, Arvina Ram for technical support, David Winter for advice on data analysis, Pierre Dupont for bioinformatics assistance, Kimberly Green for help with some of the microscopy, and Chris Schardl for providing *Epichloë* spp. sequence data.

Appendix A. Supplementary data

Supplementary data to this article can be found online at https://doi.org/10.1016/j.fgb.2022.103669.

References

Ariotti, N., Hall, T., Rae, J., Ferguson, C., McMahon, K.-A., Martel, N., Webb, R., Webb, R., Teasdale, R., Parton, R., 2015. Modular detection of GFP-labeled proteins for rapid screening by electron microscopy in cells and organisms. Dev. Cell. 35 (4), 513–525.

Audhya, A., Emr, S.D., 2003. Regulation of PI4,5P_2 synthesis by nuclear-cytoplasmic shuttling of the Mss4 lipid kinase. EMBO J. 22, 4223–4236.

Audhya, A., Foti, M., Emr, S.D., Pfeffer, S.R., 2000. Distinct roles for the yeast phosphatidylinositol 4-kinases, Stt4p and Pik1p, in secretion, cell growth, and organelle membrane dynamics. Mol. Biol. Cell. 11 (8), 2673–2689.

Baird, D., Stefan, C., Audhya, A., Weys, S., Emr, S.D., 2008. Assembly of the PtdIns 4-kinase Stt4 complex at the plasma membrane requires Ypp1 and Efr3. J. Cell Biol. 183 (6), 1061–1074.

Balla, T., 2013. Phosphoinositides: Tiny lipids wth giant impact on cell regulation. Physiol Rev. 93, 1019–1137.

Barklis, E., Staubus, A.O., Mack, A., Harper, L., Barklis, R.L., Alfadhli, A., 2018. Lipid biosensor interactions with wild type and matrix deletion HIV-1 Gag proteins. Virology. 518, 264–271.

Becker, M., Becker, Y., Green, K., Scott, B., 2016. The endophytic symbiont *Epichloë festucae* establishes an epiphyllous net on the surface of *Lolium perenne* leaves by development of an expressorium, an appressorium-like leaf exit structure. New Phytol. 211 (1), 240–254.

Becker, Y., Eaton, C.J., Brasell, E., May, K.J., Becker, M., Hassing, B., Cartwright, G.M., Reinhold, L., Scott, B., 2015. The fungal Cell-Wall Integrity MAPK cascade is crucial for hyphal network formation and maintenance of restrictive growth of *Epichloë festucae* in symbiosis with *Lolium perenne*. Mol. Plant-Microbe Interact. 28 (1), 69–85.

Becker, Y., Green, K.A., Scott, B., et al., 2018. Artificial inoculation of *Epichloë festucae* into *Lolium perenne*, and visualisation of endophytic and epiphyllous fungal growth. Bio-protocol. 8, e2990.

Bononi, A., Bonora, M., Marchi, S., Missiroli, S., Poletti, F., Giorgi, C., Pandolfi, P.P., Pinton, P., 2013. Identification of PTEN at the ER and MAMs and its regulation of $Ca^{(2+)}$ signaling and apoptosis in a protein phosphatase-dependent manner. Cell Death Differ. 20 (12), 1631–1643.

Bononi, A., Pinton, P., 2015. Study of PTEN subcellular localization. Methods. 77-78, 92–103.

Burd, C.G., Emr, S.D., 1998. Phosphatidylinositol(3)-phosphate signaling mediated by specific binding to RING FYVE domains. Mol. Cell. 2 (1), 157–162.

Byrd, A.D., Schardl, C.L., Songlin, P.J., et al., 1990. The beta-tubulin gene of *Epichloë typhina* from perennial ryegrass (*Lolium perenne*). Curr. Genet. 18, 347–354.

Chen, C.Y., Chen, J., He, L., et al., 2018. PTEN: tumor suppressor and metabolic regulator. Front. Endocrinol. (Lausanne) 9, 338.

Chujo, T., Lukito, Y., Eaton, C.J., Dupont, P.-Y., Johnson, L.J., Winter, D., Cox, M.P., Scott, B., 2019. Complex epigenetic regulation of alkaloid biosynthesis and host interaction by heterochromatin protein I in a fungal endophyte-plant symbiosis. Fungal Genet. Biol. 125, 71–83.

Chung, K.R., Schardl, C.L., 1997. Sexual cycle and horizontal transmission of the grass symbiont, *Epichloë typina*. Mycol. Res. 101, 295–301.

Cid, V.J., Rodríguez-Escudero, I., Andrés-Pons, A., Romá-Mateo, C., Gil, A., den Hertog, J., Molina, M., Pulido, R., 2008. Assessment of PTEN tumor suppressor activity in nonmammalian models: the year of the yeast. Oncogene. 27 (41), 5431–5442.

Conibear, E., Stevens, T.H., 2000. Vps52p, Vps53p, and Vps54p form a novel multisubunit complex required for protein sorting at the yeast late Golgi. Mol. Biol. Cell. 11, 305–323.

Corral-Ramos, C., Roca, M.G., Di Pietro, A., Roncero, M.I.G., Ruiz-Roldán, C., 2015. Autophagy contributes to regulation of nuclear dynamics during vegetative growth and hyphal fusion in *Fusarium oxysporum*. Autophagy. 11 (1), 131–144.

De Craene, J.-O., Bertazzi, D., Bär, S., Friant, S., 2017. Phosphoinositides, major actors in membrane trafficking and lipid signaling pathways. Int. J. Mol. Sci. 18 (3), 634. https://doi.org/10.3390/ijms18030634.

De Matteis, M.A., Wilson, C., D'Angelo, G., 2013. Phosphatidylinositol-4-phosphate: the Golgi and beyond. Bioessays. 35 (7), 612–622.

Dean, Ralph, Van kan, J.A.L., Pretorius, Z.A., Hammond-kosack, K.E., Di pietro, Antonio, Spanu, P.D., Rudd, J.J., Dickman, Marty, Kahmann, Regine, Ellis, Jeff, Foster, G.D., 2012. The top 10 fungal pathogens in molecular plant pathology. Mol. Plant Pathol. 13 (4), 414–430.

Desrivières, S., Cooke, F.T., Parker, P.J., Hall, M.N., 1998. MSS4, a phosphatidylinositol-4-phosphate 5-kinase required for organization of the actin cytoskeleton in *Saccharomyces cerevisiae*. J. Biol. Chem. 273 (25), 15787–15793.

Di Paolo, G., De Camilli, P., 2006. Phosphoinositides in cell regulation and membrane dynamics. Nature. 443 (7112), 651–657.

Di Pietro, A., García-Maceira, F.I., Méglecz, E., Roncero, M.I.G., 2001. A MAP kinase of the vascular wilt fungus *Fusarium oxysporum* is essential for root penetration and pathogenesis. Mol. Microbiol. 39 (5), 1140–1152.

Di Pietro, A., Roncero, M.I.G., 1998. Cloning, expression, and role in pathogenicity of pg1 encoding the major extracellular endopolygalacturonase of the vascular wilt pathogen *Fusarium oxysporum*. Mol. Plant-Microbe Interact. 11 (2), 91–98.

Di Pietro, A.D., Madrid, M.P., Caracuel, Z., Delgado-Jarana, J., Roncero, M.I.G., 2003. *Fusarium oxysporum*: exploring the molecular arsenal of a vascular wilt fungus. Mol. Plant Pathol. 4 (5), 315–325.

Dowler, S., Currie, R.A., Campbell, D.G., Deak, M., Kular, G., Downes, C.P., Alessi, D.R., 2000. Identification of pleckstrin-homology-domain-containing proteins with novel phosphoinositide-binding specificities. Biochem. J. 351 (1), 19–31.

Eaton, C.J., Dupont, P.-Y., Solomon, P., Clayton, W., Scott, B., Cox, M.P., 2015. A core gene set describes the molecular basis of mutualism and antagonism in *Epichloë spp*. Mol. Plant-Microbe Interact. 28 (3), 218–231.

Eaton, C.J., Jourdain, I., Foster, S.J., Hyams, J.S., Scott, B., 2008. Functional analysis of a fungal endophyte stress-activated MAP kinase. Current Genet. 53 (3), 163–174.

Echauri-Espinosa, R.O., Callejas-Negrete, O.A., Roberson, R.W., Bartnicki-García, S., Mouriño-Pérez, R.R., Bassilana, M., 2012. Coronin is a component of the endocytic collar of hyphae of *Neurospora crassa* and is necessary for normal growth and morphogenesis. PLoS One. 7 (5), e38237. https://doi.org/10.1371/journal.pone.0038237.

Falkenburger, B.H., Jensen, J.B., Dickson, E.J., et al., 2010. Phosphoinositides: lipid regulators of membrane proteins. J. Physiol. 588, 3179–3185.

Gaullier, J.-M., Rønning, E., Gillooly, D.J., Stenmark, H., 2000. Interaction of the EEA1 FYVE finger with phosphatidylinositol 3-phosphate and early endosomes. Role of conserved residues. J. Biol. Chem. 275 (32), 24595–24600.

Ghugtyal, V., Garcia-Rodas, R., Seminara, A., Schaub, S., Bassilana, M., Arkowitz, R.A., 2015. Phosphatidylinositol-4-phosphate-dependent membrane traffic is critical for fungal filamentous growth. Proc. Natl. Acad. Sci. USA 112 (28), 8644–8649.

Gibson, D.G., 2009. Synthesis of DNA fragments in yeast by one-step assembly of overlapping oligonucleotides. Nucl Acids Res. 37 (20), 6984–6990.

Gillooly, D.J., Morrow, I.C., Lindsay, M., et al., 2000. Localization of phosphatidylinositol 3-phosphate in yeast and mammalian cells. EMBO J. 19, 4577–4588.

Godi, A., Campli, A.D., Konstantakopoulos, A., Tullio, G.D., Alessi, D.R., Kular, G.S., Daniele, T., Marra, P., Lucocq, J.M., Matteis, M.A.D., 2004. FAPPs control Golgi-to-cell-surface membrane traffic by binding to ARF and PtdIns(4)P. Nat. Cell Biol. 6 (5), 393–404.

Green, K.A., 2016. A conserved signalling network regulates *Epichloë festucae* cell-cell fusion and the mutualistic symbiotic interaction between *E. festucae* and *Lolium perenne*. PhD in Genetics at Massey University, Manawatu, New Zealand.

Green, K.A., Becker, Y., Fitzsimons, H.L., Scott, B., 2016. An *Epichloë festucae* homologue of MOB3, a component of the STRIPAK complex, is required for the establishment of a mutualistic symbiotic interaction with *Lolium perenne*. Mol. Plant Pathol. 17 (9), 1480–1492.

Guillas, I., Vernay, A., Vitagliano, J.J., et al., 2013. Phosphatidylinositol 4,5-bisphosphate is required for invasive growth in *Saccharomyces cerevisiae*. J Cell Sci. 126, 3602–3614.

Hammond, G.R.V., Fischer, M.J., Anderson, K.E., Holdich, J., Koteci, A., Balla, T., Irvine, R.F., 2012. PI4P and PI(4,5)P2 are essential but independent lipid determinants of membrane identity. Science 337 (6095), 727–730.

Hanahan, D., 1983. Studies on transformation of *Escherichia coli* with plasmids. J. Mol. Biol. 166 (4), 557–580.

Hasegawa, J., Strunk, B.S., Weisman, L.S., 2017. PI5P and PI(3,5)P2: minor, but essential phosphoinositides. Cell Struct. Funct. 42, 49–60.

Hassing, B., Eaton, C.J., Winter, D., Green, K.A., Brandt, U., Savoian, M.S., Mesarich, C. H., Fleissner, A., Scott, B., 2020. Phosphatidic acid produced by phospholipase D is required for hyphal cell-cell fusion and fungal-plant symbiosis. Mol. Microbiol. 113, 1101–1121. https://doi.org/10.1111/mmi.14480.

Hassing, B., Winter, D., Becker, Y., Mesarich, C.H., Eaton, C.J., Scott, B., Wilson, R.A., 2019. Analysis of *Epichloë festucae* small secreted proteins in the interaction with *Lolium perenne*. PLoS One. 14 (2), e0209463. https://doi.org/10.1371/journal.pone.0209463.

Heit, B., Robbins, S.M., Downey, C.M., Guan, Z., Colarusso, P., Miller, B.J., Jirik, F.R., Kubes, P., 2008. PTEN functions to prioritize chemotactic cues and prevent distraction in migrating neutrophils. Nature Immunol. 9 (7), 743–752.

Heymont, J., Berenfeld, L., Collins, J., Kaganovich, A., Maynes, B., Moulin, A., Ratskovskaya, I., Poon, P.P., Johnston, G.C., Kamenetsky, M., DeSilva, J., Sun, H., Petsko, G.A., Engebrecht, J., 2000. TEP1, the yeast homolog of the human tumor suppressor gene PTEN/MMAC1/TEP1, is linked to the phosphatidylinositol pathway and plays a role in the developmental process of sporulation. Proc. Natl. Acad. Sci. USA 97 (23), 12672–12677.

Homma, K., Terui, S., Minemura, M., Qadota, H., Anraku, Y., Kanaho, Y., Ohya, Y., 1998. Phosphatidylinositol-4-phosphate 5-kinase localized on the plasma membrane is essential for yeast cell morphogenesis. J. Biol. Chem. 273 (25), 15779–15786.

Iijima, M., Devreotes, P., 2002. Tumor suppressor PTEN mediates sensing of chemoattractant gradients. Cell. 109 (5), 599–610.

Iijima, M., Huang, Y.E., Luo, H.R., Vazquez, F., Devreotes, P.N., 2004. Novel mechanism of PTEN regulation by its phosphatidylinositol 4,5-bisphosphate binding motif is critical for chemotaxis. J. Biol. Chem. 279 (16), 16606–16613.

Ischebeck, T., Stenzel, I., Heilmann, I., 2008. Type B phosphatidylinositol-4-phosphate 5-kinases mediate *Arabidopsis* and *Nicotiana tabacum* pollen tube growth by regulating apical pectin secretion. Plant Cell. 20 (12), 3312–3330.

Itoh, Y., Johnson, R., Scott, B., 1994. Integrative transformation of the mycotoxin-producing fungus, *Penicillium paxilli*. Curr. Genet. 25 (6), 508–513.

Jones, P., Binns, D., Chang, H.-Y., Fraser, M., Li, W., McAnulla, C., McWilliam, H., Maslen, J., Mitchell, A., Nuka, G., Pesseat, S., Quinn, A.F., Sangrador-Vegas, A., Scheremetjew, M., Yong, S.-Y., Lopez, R., Hunter, S., 2014. InterProScan 5: genome-scale protein function classification. Bioinformatics. 30 (9), 1236–1240.

Katoh, K., Rozewicki, J., Yamada, K.D., 2017. MAFFT online service: multiple sequence alignment, interactive sequence choice and visualization. Brief. Bioinf. 20 (4), 1160–1166.

Kavran, J.M., Klein, D.E., Lee, A., Falasca, M., Isakoff, S.J., Skolnik, E.Y., Lemmon, M.A., 1998. Specificity and promiscuity in phosphoinositide binding by pleckstrin homology domains. J. Biol. Chem. 273 (46), 30497–30508.

Kayano, Y., Tanaka, A., Takemoto, D., Wilson, R.A., 2018. Two closely related Rho GTPases, Cdc42 and RacA, of the endophytic fungus *Epichloë festucae* have contrasting roles for ROS production and symbiotic infection synchronized with the host plant. PLoS Pathog. 14 (1), e1006840. https://doi.org/10.1371/journal.ppat.1006840.

Kimber, W.A., Trinkle-mulcahy, L., Cheung, P.C.F., Deak, M., Marsden, L.J., Kieloch, A., Watt, S., Javier, R.T., Gray, A., Downes, C.P., Lucocq, J.M., Alessi, D.R., 2002. Evidence that the tandem-pleckstrin-homology-domain-containing protein TAPP1 interacts with Ptd(3,4)P_2 and the multi-PDZ-domain-containing protein MUPP1 *in vivo*. Biochem. J. 361 (3), 525–536.

König, S., Hoffmann, M., Mosblech, A., Heilmann, I., 2008. Determination of content and fatty acid composition of unlabeled phosphoinositide species by thin-layer chromatography and gas chromatography. Anal. Biochem. 378 (2), 197–201.

Kosugi, S., Hasebe, M., Entani, T., et al., 2008. Design of peptide inhibitors for the importin alpha/beta nuclear import pathway by activity-based profiling. Chem. Biology. 15, 940–949.

Kosugi, S., Hasebe, M., Matsumura, N., et al., 2009a. Six classes of nuclear localization signals specific to different binding grooves of importin alpha. J. Biol. Chem. 284, 478–485.

Kosugi, S., Hasebe, M., Tomita, M., Yanagawa, H., 2009b. Systematic identification of cell cycle-dependent yeast nucleocytoplasmic shuttling proteins by prediction of composite motifs. Proc. Natl. Acad. Sci. USA 106 (25), 10171–10176.

Latch, G.C.M., Christensen, M.J., 1985. Artificial infection of grasses with endophytes. Annals Appl. Biol. 107 (1), 17–24.

Lee, J.-O., Yang, H., Georgescu, M.-M., Di Cristofano, A., Maehama, T., Shi, Y., Dixon, J. E., Pandolfi, P., Pavletich, N.P., 1999. Crystal structure of the PTEN tumor suppressor: implications for its phosphoinositide phosphatase activity and membrane association. Cell. 99 (3), 323–334.

Li, X., Wang, X., Zhang, X., Zhao, M., Tsang, W.L., Zhang, Y., Yau, R.G.W., Weisman, L.S., Xu, H., 2013. Genetically encoded fluorescent probe to visualize intracellular phosphatidylinositol 3,5-bisphosphate localization and dynamics. Proc. Natl. Acad. Sci. USA 110 (52), 21165–21170.

Liaw, D., Marsh, D.J., Li, J., Dahia, P.L.M., Wang, S.I., Zheng, Z., Bose, S., Call, K.M., Tsou, H.C., Peacoke, M., Eng, C., Parsons, R., 1997. Germline mutations of the PTEN gene in Cowden disease, an inherited breast and thyroid cancer syndrome. Nat. Genet. 16 (1), 64–67.

Liu, D., Coloe, S., Baird, R., Pedersen, J., 2000. Rapid mini-preparation of fungal DNA for PCR. J. Clin. Microbiol. 38 (1), 471.

Lukito, Y., Chujo, T., Scott, B., 2015. Molecular and cellular analysis of the pH response transcription factor PacC in the fungal symbiont *Epichloë festucae*. Fungal Genet. Biol. 85, 25–37.

Mähs, A., Ischebeck, T., Heilig, Y., Stenzel, I., Hempel, F., Seiler, S., Heilmann, I., Herrera-Estrella, A., 2012. The essential phosphoinositide kinase MSS-4 is required for polar hyphal morphogenesis, localizing to sites of growth and cell fusion in *Neurospora crassa*. PLoS One. 7 (12), e51454. https://doi.org/10.1371/journal.pone.0051454.

Manning, B.D., Cantley, L.C., 2007. AKT/PKB signaling: navigating downstream. Cell 129 (7), 1261–1274.

Marat, A.L., Haucke, V., 2016. Phosphatidylinositol 3-phosphates-at the interface between cell signalling and membrane traffic. EMBO J. 35 (6), 561–579.

McCartney, A.J., Zhang, Y., Weisman, L.S., 2014. Phosphatidylinositol 3,5-bisphosphate: low abundance, high significance. Bioessays. 36 (1), 52–64.

McInnes, R., Lidgett, A., Lynch, D., Huxley, H., Jones, E., Mahoney, N., Spangenberg, G., 2002. Isolation and characterization of a cinnamoyl-CoA reductase gene from perennial ryegrass (*Lolium perenne*). J. Plant Physiol. 159 (4), 415–422.

Mitra, P., Zhang, Y., Rameh, L.E., Ivshina, M.P., McCollum, D., Nunnari, J.J., Hendricks, G.M., Kerr, M.L., Field, S.J., Cantley, L.C., Ross, A.H., 2004. A novel phosphatidylinositol(3,4,5)P_3 pathway in fission yeast. J. Cell Biol. 166 (2), 205–211.

Nguyen, H.N., Afkari, Y., Senoo, H., Sesaki, H., Devreotes, P.N., Iijima, M., 2014. Mechanism of human PTEN localization revealed by heterologous expression in Dictyostelium. Oncogene 33 (50), 5688–5696.

Putz, U., Howitt, J., Doan, A., Goh, C.-P., Low, L.-H., Silke, J., Tan, S.-S., 2012. The tumor suppressor PTEN is exported in exosomes and has phosphatase activity in recipient cells. Sci Signal. 5 (243) https://doi.org/10.1126/scisignal.2003084.

Rameh, L.E., Arvidsson, A.-K., Carraway, K.L., Couvillon, A.D., Rathbun, G., Crompton, A., VanRenterghem, B., Czech, M.P., Ravichandran, K.S., Burakoff, S.J., Wang, D.-S., Chen, C.-S., Cantley, L.C., 1997. A comparative analysis of the phosphoinositide binding specificity of pleckstrin homology domains. J. Biol. Chem. 272 (35), 22059–22066.

Salim, K., Bottomley, M.J., Querfurth, E., Zvelebil, M.J., Gout, I., Scaife, R., Margolis, R. L., Gigg, R., Smith, C.I., Driscoll, P.C., Waterfield, M.D., Panayotou, G., 1996. Distinct specificity in the recognition of phosphoinositides by the pleckstrin homology domains of dynamin and Bruton's tyrosine kinase. EMBO J. 15 (22), 6241–6250.

Schardl, C.L., 2001. *Epichloë festucae* and related mutualistic symbionts of grasses. Fungal Genet. Biol. 33 (2), 69–82.

Schardl, C.L., Young, C.A., Hesse, U., Amyotte, S.G., Andreeva, K., Calie, P.J., Fleetwood, D.J., Haws, D.C., Moore, N., Oeser, B., Panaccione, D.G., Schweri, K.K., Voisey, C.R., Farman, M.L., Jaromczyk, J.W., Roe, B.A., O'Sullivan, D.M., Scott, B.,

Tudzynski, P., An, Z., Arnaoudova, E.G., Bullock, C.T., Charlton, N.D., Chen, L.i., Cox, M., Dinkins, R.D., Florea, S., Glenn, A.E., Gordon, A., Güldener, U., Harris, D.R., Hollin, W., Jaromczyk, J., Johnson, R.D., Khan, A.K., Leistner, E., Leuchtmann, A., Li, C., Liu, JinGe, Liu, J., Liu, M., Mace, W., Machado, C., Nagabhyru, P., Pan, J., Schmid, J., Sugawara, K., Steiner, U., Takach, J.E., Tanaka, E., Webb, J.S., Wilson, E. V., Wiseman, J.L., Yoshida, R., Zeng, Z., Heitman, J., 2013. Plant-symbiotic fungi as chemical engineers: multi-genome analysis of the *Clavicipitaceae* reveals dynamics of alkaloid loci. PLoS Genet. 9 (2), e1003323. https://doi.org/10.1371/journal.pgen.1003323.

Scott, B., Schardl, C., 1993. Fungal symbionts of grasses: evolutionary insights and agricultural potential. Trends Microbiol. 1 (5), 196–200.

Segorbe, D., Di Pietro, A., Pérez-Nadales, E., Turrà, D., 2017. Three *Fusarium oxysporum* mitogen-activated protein kinases (MAPKs) have distinct and complementary roles in stress adaptation and cross-kingdom pathogenicity. Mol. Plant Pathol. 18 (7), 912–924.

Taheri-Talesh, N., Horio, T., Araujo-Bazán, L., Dou, X., Espeso, E.A., Peñalva, M.A., Osmani, S.A., Oakley, B.R., Drubin, D., 2008. The tip growth apparatus of *Aspergillus nidulans*. Mol. Biol. Cell. 19 (4), 1439–1449.

Tanaka, A., Christensen, M.J., Takemoto, D., Park, P., Scott, B., 2006. Reactive oxygen species play a role in regulating a fungus-perennial ryegrass mutualistic interaction. Plant Cell. 18 (4), 1052–1066.

Turrà, D., El Ghalid, M., Rossi, F., Di Pietro, A., 2015. Fungal pathogen uses sex pheromone receptor for chemotropic sensing of host plant signals. Nature. 527 (7579), 521–524.

van Leeuwen, W., Vermeer, J.E.M., Gadella, T.W.J., Munnik, T., 2007. Visualization of phosphatidylinositol 4,5-bisphosphate in the plasma membrane of suspension-cultured tobacco BY-2 cells and whole *Arabidopsis* seedlings. Plant J. 52 (6), 1014–1026.

Várnai, P., Lin, X., Lee, S.B., Tuymetova, G., Bondeva, T., Spät, A., Rhee, S.G., Hajnóczky, G., Balla, T., 2002. Inositol lipid binding and membrane localization of isolated pleckstrin homology (PH) domains. Studies on the PH domains of phospholipase C delta 1 and p130. J. Biol. Chem. 277 (30), 27412–27422.

Vazquez, F., Matsuoka, S., Sellers, W.R., Yanagida, T., Ueda, M., Devreotes, P.N., 2006. Tumor suppressor PTEN acts through dynamic interaction with the plasma membrane. Proc. Natl. Acad. Sci. USA 103 (10), 3633–3638.

Vermeer, J.E.M., Thole, J.M., Goedhart, J., Nielsen, E., Munnik, T., Gadella Jr, T.W.J., 2009. Imaging phosphatidylinositol 4-phosphate dynamics in living plant cells. Plant J. 57 (2), 356–372.

Vermeer, J.E.M., van Leeuwen, W., Tobeña-Santamaria, R., Laxalt, A.M., Jones, D.R., Divecha, N., Gadella, T.W.J., Munnik, T., 2006. Visualization of PtdIns3P dynamics in living plant cells. Plant J. 47 (5), 687–700.

Vernay, A., Schaub, S., Guillas, I., Bassilana, M., Arkowitz, R.A., 2012. A steep phosphoinositide bis-phosphate gradient forms during fungal filamentous growth. J. Cell Biol. 198 (4), 711–730.

Vijayakrishnapillai, L., Desmarais, J., Groeschen, M., Perlin, M., 2018. Deletion of *ptn1*, a PTEN/TEP1 orthologue, in *Ustilago maydis* reduces pathogenicity and teliospore development. J. Fungi (Basel) 5 (1), 1. https://doi.org/10.3390/jof5010001.

Walker, S.M., Leslie, N.R., Perera, N.M., Batty, I.H., Downes, C.P., 2004. The tumour-suppressor function of PTEN requires an N-terminal lipid-binding motif. Biochem. J. 379 (2), 301–307.

Weiger, M.C., Parent, C.A., 2012. Phosphoinositides in chemotaxis. Subcell. Biochem. 59, 217–254.

Wilkinson, H.H., Siegel, M.R., Blankenship, J.D., Mallory, A.C., Bush, L.P., Schardl, C.L., 2000. Contribution of fungal loline alkaloids to protection from aphids in a grass-endophyte mutualism. Mol. Plant-Microbe Interact. 13 (10), 1027–1033.

Yamamoto, W., Wada, S., Nagano, M., et al., 2018. Distinct roles for plasma membrane PtdIns(4)P and PtdIns(4,5)P_2 during receptor-mediated endocytosis in yeast. J. Cell Sci. 131, jcs207696.

Yoshida, S., Ohya, Y., Nakano, A., Anraku, Y., 1994. Genetic interactions among genes involved in the STT4-PKC1 pathway of *Saccharomyces cerevisiae*. Mol. Gen. Genet. 242 (6), 631–640.

Young, C.A., Bryant, M.K., Christensen, M.J., Tapper, B.A., Bryan, G.T., Scott, B., 2005. Molecular cloning and genetic analysis of a symbiosis-expressed gene cluster for lolitrem biosynthesis from a mutualistic endophyte of perennial ryegrass. Mol. Gen. Genet. 274 (1), 13–29.

Zhang, Dajun, Fan, Feiyu, Yang, Jingran, Wang, Xuli, Qiu, Dewen, Jiang, Linghuo, 2010. FgTep1p is linked to the phosphatidylinositol-3 kinase signalling pathway and plays a role in the virulence of *Fusarium graminearum* on wheat. Mol. Plant Pathol. 11 (4), 495–502.

Zhu, Y., Wloch, A., Wu, Q., Peters, C., Pagenstecher, A., Bertalanffy, H., Sure, U., 2009. Involvement of PTEN promoter methylation in cerebral cavernous malformations. Stroke. 40 (3), 820–826.